7-2009

Paragneiss Zircon Geochronology and Trace Element Geochemistry, North Qaidam HP/UHP Terrane, Western China

Chris G. Mattinson
Central Washington University, mattinson@geology.cwu.edu

Joseph L. Wooden
U.S. Geological Survey

Jian-Xin Zhang
Chinese Academy of Geological Sciences, Institute of Geology

D. K. Bird
Stanford University

Recommended Citation
Mattinson, C.G. , Wooden, J.L., Zhang, J.X., & Bird, D.K. (2009). Paragneiss zircon geochronology and trace element geochemistry, North Qaidam HP/UHP Terrane, Western China. *Journal of Asian Earth Sciences,* 35, 298-309. DOI: 10.1016/j.jseaes.2008.12.007

Citation: Mattinson, C.G., Wooden, J.L., Zhang, J.X., and Bird, D.K. (2009) Paragneiss zircon geochronology and trace element geochemistry, North Qaidam HP/UHP terrane, western China. Journal of Asian Earth Sciences, 35, 298-309.

Paragneiss zircon geochronology and trace element geochemistry, North Qaidam HP/UHP terrane, western China

C.G. Mattinson, J. L. Wooden, J.X. Zhang, and D.K. Bird

Citation: Mattinson, C.G., Wooden, J.L., Zhang, J.X., and Bird, D.K. (2009) Paragneiss zircon geochronology and trace element geochemistry, North Qaidam HP/UHP terrane, western China. Journal of Asian Earth Sciences, 35, 298-309.

Paragneiss zircon geochronology and trace element geochemistry, North Qaidam HP/UHP terrane, western China

C.G. Mattinson[a,d*], J. L. Wooden[b], J.X. Zhang[c], and D.K. Bird[d]

[a]Dept. of Geological Sciences, Central Washington University,

400 E. University Way, Ellensburg, WA 98926, USA

[b]U.S. Geological Survey, 345 Middlefield Road, Menlo Park, CA 94025, USA

[c]Chinese Academy of Geological Sciences, Institute of Geology, Beijing 100037, China

[d]Dept. of Geological & Environmental Sciences, Stanford University, Stanford, CA 94305, USA

Abstract

In the southeastern part of the North Qaidam terrane, near Dulan, paragneiss hosts minor peridotite and UHP eclogite. Zircon geochronology and trace element geochemistry of three paragneiss samples (located within a ~3 km transect) indicates that eclogite facies metamorphism resulted in variable degrees of zircon growth and recrystallization in the three samples. Inherited zircon core age groups at 1.8 and 2.5 Ga suggest that the protoliths of these rocks may have received sediments from the Yangtze or North China cratons. Mineral inclusions, depletion in HREE, and absence of negative Eu anomalies indicate that zircon U-Pb ages of 431 ± 5 Ma and 426 ± 4 Ma reflect eclogite-facies zircon growth in two of the samples. Ti-in-zircon thermometry results are tightly grouped at ~660 °C and ~600 °C, respectively. Inclusions of metamorphic minerals, scarcity of inherited cores, and lack of isotopic or trace element inheritance demonstrate that significant new metamorphic zircon growth must have occurred. In contrast, zircon in the third sample is dominated by inherited grains, and rims show isotopic and

* Corresponding author. Tel.: +1-509-963-1628; fax: +1-509-963-2821. E-mail address: mattinson@geology.cwu.edu.

trace element inheritance, suggesting solid-state recrystallization of detrital zircon with only minor new growth.

1. Introduction

Ultra-high pressure (UHP) metamorphism, defined by the pressure-temperature conditions of the coesite stability field (P > 27 kbar, depths > 80 km), is a product of continental subduction and collision (Chopin, 2003; Coleman and Wang, 1995). Of the more than 20 UHP localities known (e.g., Liou et al., this issue), protracted (U)HP metamorphism and/or multiple (U)HP metamorphic events are documented in several localities including Norway (Brueckner and Van Roermund, 2004; Hacker, 2007; Kylander-Clark et al., 2007), Greenland (McClelland et al., 2006), the Alps (Lapen et al., 2003; Rubatto and Scambelluri, 2003), the Greek Rhodope (Liati, 2005), western China (Mattinson et al., 2006b; Song et al., 2006), and eastern China (Ratschbacher et al., 2003; Wan et al., 2005). To determine the rates and durations of UHP processes, it is important to understand how minerals of geochronologic significance, such as zircon, record complex metamorphic histories. Western China contains several high-pressure (HP) metamorphic belts; evidence for UHP metamorphism has been documented from the North Qaidam and South Altyn terranes (Fig. 1; Liu et al., 2002; Song et al., 2003a,b, 2005; Yang et al., 2001a; J.X. Zhang et al., 2002; see Mattinson et al., 2007a for a review). Here we present zircon U-Pb geochronology, trace element geochemistry including Ti-in-zircon thermometry, Raman analysis of inclusions in zircon, and trace element geochemistry of garnet to document the age and P-T significance of zircon growth in three samples of eclogite-hosting paragneiss from the Dulan region, southeastern North Qaidam HP/UHP terrane.

2. Geologic setting of the North Qaidam terrane

The northwest-southeast trending North Qaidam terrane records Early Paleozoic continental collision, and exposures are bounded on the southwest by the Qaidam Basin, and on the northeast by the Qilian terrane (Fig. 1; Mattinson et al., 2007a; J.S. Yang et al., 2001b). The basement of the North Qaidam terrane is the Proterozoic Dakendaban Group gneiss, which is overlain by Paleozoic metasediments, and intruded by granitoids. The Dakendaban Group is dominated by granitic orthogneiss and paragneiss of variable composition, with minor marble, amphibolite, migmatite, and locally eclogite and garnet peridotite (J.J. Yang and Deng, 1994; J.S. Yang et al., 2001b; Mattinson et al., 2007a). Lu et al. (2002) have recently proposed a revision to the nomenclature of the Dakendaban Group; UHP rocks of the Dulan area include their unnamed Neoproterozoic metagranitic gneiss as well as the metasedimentary Shaliuhe Group.

The original contact relationship (depositional, intrusive, tectonic) between ortho- and paragneiss is unclear, but field relations, including inclusions of paragneiss in granitic orthogneiss (Wan et al., 2006) and intercalation of ortho- and paragneiss, suggest that the (meta)sedimentary protoliths of the paragneiss were intruded by the granite (now orthogneiss), which has been dated at ca. 900-1000 Ma (Gehrels et al., 2003b; Mattinson et al., 2006a; Wan et al., 2001; J.X. Zhang et al., 2008). Evidence of Proterozoic (ca. 900 Ma, approximately the same age as the granites) metamorphism in paragneiss samples from Xitie Shan (J.X. Zhang et al., 2008) and Dulan (Mattinson et al., 2007b) also suggest that the protoliths of some paragneisses were deposited prior to granite intrusion, and intrusion of the granites may have been accompanied by metamorphism of the adjacent sediments. It is unclear if previously documented <1 Ga zircon implies that some paragneiss protoliths have a depositional age <1 Ga

(Song et al., 2006; J.S. Yang et al., 2005), or if these ages reflect Proterozoic metamorphism (J.X. Zhang et al., 2008). Neodymium depleted-mantle model ages from the paragneiss are predominantly 1.9–2.2 Ga (Wan et al., 2006), and should approximate the formation age of the parent rocks from which the sediments were derived. This suggests the sediments were derived from Paleoproterozoic ± Archean crustal material, consistent with analyses of zircon cores from paragneiss (see below; Mattinson et al., 2007a); a passive margin depositional environment is suggested by Wan et al. (2006), consistent with the occurrence of marble and metamorphosed equivalents of mature sediments (e.g., biotite quartzite).

Eclogite occurs over a distance of 350 km in the Lüliang Shan, Xitie Shan, and near Dulan (Figs. 1 and 2). The eclogite and peridotite occur as blocks, boudins or layers in the host para- and orthogneiss, and typically are 10s to <1 m across, but locally are >100 m. Zircon U-Pb ages from gneiss, eclogite, and peridotite of the North Qaidam terrane have been interpreted to record peak metamorphism between 497–423 Ma, similar to Sm-Nd garnet–omphacite–whole-rock isochron ages from eclogite (Mattinson et al., 2006b; Menold et al., in review; Song et al., 2003a, 2005, 2006; J.X. Zhang et al., 2005b; G. Zhang et al., 2008).

Granitoids cross-cut the regional foliation, and crystallized between 456–397 Ma, which is thought to be coeval with continental collision between the North Qaidam and Qilian terranes (Gehrels et al., 2003a; Wu et al., 2001, 2004). North of the North Qaidam terrane, granites in the southern Qilian terrane (Fig. 1) have I-type geochemistry, 496–425 Ma ages, and are interpreted to represent arc magmatism (Gehrels et al., 2003a; Wu et al., 2001). The subduction polarity responsible for convergence, magmatism, and subsequent collision of the North Qaidam and Qilian terranes is unclear, and models involving both north-dipping subduction (Song et al., 2006; J.S. Yang et al., 2001b, 2002; Yin and Harrison, 2000) and south-dipping subduction

(Gehrels et al., 2003a, b; Yin et al., 2007) have been proposed (for a review, see Mattinson et al., 2007a). Additional field and geochronological work is required to resolve this problem.

3. Geology of the Dulan area

This region is named for the town of Dulan, located approximately 30 km southwest of the map area in Fig. 2. Eclogite and ultramafic rocks occur within granitic and metasedimentary gneiss both north and south of the Shaliu River. An amphibolite-facies foliation in the gneiss strikes northwest, and dips steeply northeast, modified by tight to isoclinal folds. A locally developed subhorizontal to shallowly northwest plunging lineation trends northwest. Layers and boudins of eclogite and ultramafic rocks, typically <1 to 10s of m long, but locally >100 m, are enclosed in both ortho- and paragneiss, and are aligned with the foliation in the surrounding gneiss; where developed, foliation within the layers is also concordant with the surrounding gneiss.

Granitic orthogneiss, commonly distinguished by cm-size augen, is interlayered with paragneiss at 10s–100s of meter scale and both rock types share a common foliation. Zircon U-Pb geochronology from granitic orthogneiss near Dulan indicates magmatic crystallization at ca. 925 Ma, and ages from zircon rims (618–397 Ma) are compatible with minor recrystallization during in situ Ordovician-Silurian metamorphism (Mattinson et al., 2006a). U-Pb dating of metamorphic zircon in paragneiss yields 452–423 Ma; one coesite-bearing paragneiss yields a weighted mean age of 423 ± 6 Ma (Song et al., 2006), and individual SHRIMP analyses of coesite-bearing zircon from two samples yield 427 ± 4 Ma, 439 ± 3 Ma, and 440 ± 17 Ma (J.S. Yang et al., 2005).

Song et al. (2003a, b) report peak P-T conditions for eclogites of 29–33 kbar, 631–746 °C. The discovery of coesite included in zircon from the host paragneiss confirms that both the

mafic/ultramafic rocks and the felsic host gneiss were metamorphosed at UHP conditions (Song et al., 2003a, 2003b, 2006; J.S. Yang et al., 2001a, 2005). Zircon U-Pb and Sm-Nd isochron ages of eclogites are 459–422 Ma. Inclusions and REE patterns indicate that these ages represent eclogite-facies growth (Mattinson et al., 2006b; Song et al., 2003a, 2006; G. Zhang et al., 2008).

Retrograde amphibolite-facies conditions recorded in retrogressed eclogites are 7–9 kbar, 660–695 °C (Song et al., 2003b). Constraints on the timing of retrograde metamorphism and exhumation include zircon rim ages from eclogite (426 ± 12 Ma, n = 1) and gneiss (403 ± 9 Ma, n = 6; 419 ± 7 Ma, n = 1), and a 402 Ma muscovite $^{40}Ar/^{39}Ar$ age (Song et al., 2006; Yang et al., 2005). These results suggest the UHP rocks reached mid- to shallow crustal levels at or before this time. The undeformed, cross-cutting granite and granodiorite of the Yematan batholith (Fig. 2) indicates that ductile deformation ceased before crystallization of the batholith at 397 ±3 Ma (Wu et al., 2001, 2004).

4. Sample description

Three paragneiss samples were collected for analysis (Fig. 2). Paragneiss ZD21G (collected at N36° 36.25′, E98°28.44′) has a well-developed schistosity due to abundant, coarse-grained muscovite, and contains 2-3 cm tourmaline in outcrop. This sample contains sparse (<5 vol%), rounded 1-5 mm garnet, muscovite, tourmaline, plagioclase (partially sericitized), and quartz, with minor biotite, K-feldspar, rutile (inclusions in garnet, but sparse in the matrix), ilmenite, zircon, monazite, apatite, and secondary chlorite. The outcrop of paragneiss D12H (collected at N36° 36.56′, E98°27.36′) contains small layers and lenses of amphibolite and K-feldspar-rich layers similar to orthogneiss. This sample contains sparse (<5 vol%), rounded 1-5 mm garnet, muscovite, tourmaline, plagioclase, and quartz, with minor biotite, rutile (only as

inclusions in garnet), ilmenite (in the matrix), zircon, and secondary chlorite. Paragneiss ZD22A (collected at N36° 36.06′, E98°28.76′) contains abundant quartz and biotite, with minor muscovite, K-feldspar, strongly sericitized plagioclase, opaques, zircon, and apatite; garnet is absent.

5. Analytical methods

Zircon U-Pb geochronology and trace element analyses were performed in separate analytical sessions using the Stanford/USGS SHRIMP-RG (sensitive high-resolution ion micro-probe reverse geometry) facility. Zircon grains were mounted in a 2.54 cm epoxy disc and polished to approximate half-sections prior to reflected light and cathodoluminescence (CL) imaging. Cathodoluminescence images were collected using a JEOL 5600LV scanning electron microscope. Locations of SHRIMP analyses were chosen to avoid cracks, pits, or inclusions identified in CL and reflected light images. The sample was Au-coated, and placed under high vacuum for 24 hr prior to analysis to minimize interference from gas species.

The analytical routine for U-Pb geochronology followed Williams (1998), and age calculations were performed using the Isoplot and Squid programs (Ludwig, 2001, 2003) and IUGS recommended decay constants (Steiger and Jäger, 1977). The sample was sputtered by a ~5 nA O_2^- primary beam focused to ~30 μm diameter, and the mass resolution was 6000–7000 at 10% peak height. Prior to analysis, the primary ion beam was rastered across the grain surface to remove the Au-coating and any surface contamination. Each analysis comprised 6 scans of peaks corresponding to $^{90}Zr_2{}^{16}O$, ^{204}Pb, background, ^{206}Pb, ^{207}Pb, ^{208}Pb, ^{238}U, $^{232}Th^{16}O$ and $^{238}U^{16}O$, with count times of 2–20 s for each peak. The concentration of U was calibrated using zircon standard CZ3, and the Pb/U ratio was calibrated using zircon age standard R33 (419 Ma; Black

et al., 2004). Estimates of common Pb compositions use the two-stage Pb evolution model of Stacey and Kramers (1975). Individual ages reported below are $^{206}Pb/^{238}U$ ages corrected for common Pb using ^{207}Pb ($^{207}Pb/^{206}Pb$ ages are corrected for common Pb using ^{204}Pb for ages >1 Ga). Ages calculated from multiple analyses are expressed as concordia ages (Ludwig, 1998) corrected for common Pb using ^{204}Pb, and errors are given at 95% confidence.

For trace element analyses, we selected one isotope to represent each element, based on abundance and absence of significant interferences, similar to the approach of Maas et al. (1992). Each analysis comprised 2 scans of peaks corresponding to ^{9}Be, ^{11}B, ^{19}F, ^{27}Al, ^{30}Si, ^{31}P, ^{32}S, ^{35}Cl, ^{40}Ca, ^{45}Sc, ^{48}Ti, ^{49}Ti, ^{51}V, ^{55}Mn, ^{56}Fe, ^{74}Ge, ^{89}Y, ^{93}Nb, $^{94}Zr^{1}H$, ^{96}Zr, ^{139}La, ^{140}Ce, ^{146}Nd, ^{147}Sm, ^{153}Eu, ^{165}Ho, $^{157}Gd^{16}O$, $^{159}Tb^{16}O$, $^{163}Dy^{16}O$, $^{166}Er^{16}O$, $^{169}Tm^{16}O$, $^{172}Yb^{16}O$, $^{175}Lu^{16}O$, $^{90}Zr_2{}^{16}O$, $^{180}Hf^{16}O$, ^{206}Pb, $^{232}Th^{16}O$, and $^{238}U^{16}O$, with count times of 2–10 s for each peak. Operating at ~11000 mass resolution at 10% peak height, these peaks are well resolved from LREE oxides and Zr, Si, O molecules, including interferences of $^{90}Zr^{+2}$ on $^{45}Sc^{+}$, $^{96}Zr^{+2}$ on $^{48}Ti^{+}$, and $^{92}Zr^{1}H$ on $^{93}Nb^{+}$, but due to the unresolved interference of $^{140}Ce^{1}H$, Pr is interpolated ($Pr^{*} = La_n^{0.33} \times Nd_n^{0.67}$). Primary beam current and spot size were similar to those used for geochronology. The raw data were converted to ppm by normalizing average count rates to ^{30}Si, and calibrating concentrations to trace element values for zircon standard CZ3 (Mazdab and Wooden, 2006, in review). Conversion of these concentrations to chondrite-normalized patterns (Coryell et al., 1963) uses the recommended CI carbonaceous chondrite composition of McDonough and Sun (1995). Chondrite-normalized concentrations are indicated by a subscripted "n".

Ti-in-zircon thermometry (Watson et al., 2006; Ferry and Watson, 2007) assumes TiO_2 and SiO_2 activities = 1.0, which is appropriate for the quartz and rutile bearing metamorphic assemblages observed in thin section, but likely underestimates temperatures for inherited grains.

Based on 40 analyses of CZ3, standard deviations of P, Y, Hf, Th, and U are 5–10%, and the REE are 10–15%, except for La (32%) which has an extremely low abundance, providing a conservative estimate of the uncertainty of the trace element analyses (Mattinson et al., 2006b). The consistency of the REE patterns suggests that part of this variability reflects true heterogeneity in the CZ3 standard. The agreement between U concentrations measured during U-Pb analysis and trace element analysis indicates that the trace element measurements may be applied to the interpretation of the U-Pb measurements for most analyses (Tables 1 and 2). A subset of the trace element analyses contain elevated Al, Ca, Fe, Mn, and/or Cl, and are considered unrepresentative of igneous or metamorphic growth compositions (Table 2). These elements are normally very low in crystalline, inclusion-free zircon, suggesting that the elevated LREE and Ti (Table 2) of these analyses are related to mineral or fluid microinclusions, or post-crystallization introduction of these elements into radiation-damaged zones in zircon (many of these grains appear cloudy in transmitted light); Cl may have been introduced during HCl washing of the mount prior to analysis.

Mineral inclusions in zircon were identified using laser Raman spectroscopy and EMP analysis. Electron microprobe methods follow Mattinson et al. (2006b). Raman analyses were performed at the Key Laboratory for Continental Dynamics, Ministry of Land and Resources of China, Beijing, with a Renishow-1000 laser Raman spectroscope using the 514.5 nm line of an Ar-ion laser.

Following petrographic and electron microprobe investigations, major mineral trace element data were collected from thin sections at the University of California, Davis using an Agilent 7500a inductively coupled plasma mass spectrometer coupled with a Nd:YAG New Wave UP 213 nm laser ablation system. The laser was operated with a spot size of 60 μm at 10

Hz and 70% power (11.3 J/cm^2, 0.319 nJ total power), resulting in an approximate 1μm/s ablation rate. A mixed He-Ar carrier gas (He, 0.85 L/min; Ar ~1.1 L/min) was used to transport the ablation products to the mass spectrometer. Data are collected in a time-resolved mode, which includes 30 seconds of background signal, the sample signal (30 seconds, 0.01–0.05 seconds per peak), and washout (90 seconds). Peaks selected are: ^{7}Li, ^{25}Mg, ^{43}Ca, ^{45}Sc, ^{47}Ti, ^{51}V, ^{53}Cr, ^{85}Rb, ^{88}Sr, ^{89}Y, ^{90}Zr, ^{93}Nb, ^{137}Ba, ^{139}La, ^{140}Ce, ^{141}Pr, ^{146}Nd, ^{147}Sm, ^{153}Eu, ^{157}Gd, ^{159}Tb, ^{163}Dy, ^{165}Ho, ^{166}Er, ^{169}Tm, ^{172}Yb, ^{175}Lu, and ^{178}Hf. Contamination from inclusions, fractures and zones of different composition was detected by monitoring potential contaminant elements and integrating only the relevant part of the signal. Ca concentration measured by electron microprobe (JEOL 733A Superprobe at Stanford University; operating conditions as in Mattinson et al., 2004) was used as the internal standard (Table 3). USGS BCR-2G glass was used as the primary external standard (standard deviations are 3-6%, 1σ), and USGS BHVO-2G and NIST-612 glass were used as secondary standards to evaluate accuracy (generally better than 15%; compositions from USGS and Pearce et al., 1997).

6. Results

6.1 Paragneiss ZD21G

Most zircons from paragneiss ZD21G are unzoned or subtly mottled in CL (Fig. 3a, analyses 1, 25, 27), with dark to medium brightness. Sparse grains contain oscillatory zoned, bright CL cores (Fig. 3a, analysis 4), surrounded by rims with the same CL characteristics as the dominant population. Eleven analyses of the medium and dark CL grains and rims yield 152-1177 ppm U, 1-8 ppm Th, Th/U = 0.003-0.025 (Table 1), and yield a concordia age of 426 ± 4 Ma (Fig. 3c; MSWD = 1.2, probability of equivalence = 0.24, probability of concordance =

0.426). Five additional analyses of medium and dark CL grains yield 362-1586 ppm U, 1-77 ppm Th, Th/U = 0.003-0.050, and yield variably younger ages that we interpret to reflect minor Pb-loss (Fig. 3c, Table 1). Of a total of 27 trace element analyses, 15 contain elevated levels of contaminant elements (Fig. 3a, Table 2). The remaining REE patterns are characterized by flat HREE slopes (Yb_n/Gd_n = 1.8-3.6), and Eu anomalies are small ($Eu/Eu^* = Eu_n/[Sm_n \times Gd_n]^{0.5}$ = 0.63-0.78; Fig. 3a, Table 2). Ti-in-zircon thermometry (Watson et al., 2006; Ferry and Watson, 2007) yields well-grouped results of 580-620 °C, with one outlier at 693 °C (Fig. 3d, Table 2). Electron microprobe and laser Raman analysis of the sparse inclusions identified garnet, phengite, rutile, graphite, apatite, and one quartz inclusion.

Three analyses of bright CL cores reveal 152-532 ppm U, 64-198 ppm Th, Th/U = 0.38-0.98, and 1.03-2.46 Ga $^{207}Pb/^{206}Pb$ minimum ages (Table 1). The youngest age is more discordant (54%) than the two older ages (25-28%). Of four trace element analyses, two contain elevated levels of contaminant elements. The remaining REE patterns are characterized by steep HREE slopes (Yb_n/Gd_n = 15-20), and prominent negative Eu anomalies (Eu/Eu* = 0.17-0.29; Fig. 3a, Table 2). Ti-in-zircon thermometry (Watson et al., 2006; Ferry and Watson, 2007) yields 701-797 °C (Fig. 3d, Table 2). Electron microprobe and laser Raman analysis of the sparse inclusions identified quartz and apatite.

Garnet is zoned, from a Mn-rich core ($Alm_{73}Sps_7Prp_8Grs_{12}$; mineral abbreviations after Kretz, 1983), to a Ca-richer zone near the rim ($Alm_{66}Sps_2Prp_{12}Grs_{20}$), to an outermost rim similar to the core composition ($Alm_{75}Sps_6Prp_8Grs_{11}$). Trace elements are prominently zoned (Fig. 3b, Table 3), especially HREE, from core (Eu/Eu* = 0.61, Yb_n/Gd_n = 195) to rim (Eu/Eu* = 0.79, Yb_n/Gd_n = 1.7). Two garnet inclusions in zircons analyzed by EMP are compositionally similar to the Ca-rich and outermost rim compositions measured in thin section. Plagioclase includes

both albite (An_3) and oligoclase (An_{20}); a single trace element analysis of oligoclase reveals a prominent positive Eu anomaly (Eu/Eu* = 62; Fig. 3b, Table 3). K-feldspar is Ca-free, and contains low Na (Ab_1). Muscovite is zoned from more phengitic cores (Si p.f.u. = 3.20-3.25) to lower Si rims (Si p.f.u. = 3.10). One muscovite inclusion in zircon analyzed by EMP is compositionally similar to the cores of matrix muscovite analyzed in thin section.

6.2 Paragneiss D12H

Most zircons from paragneiss D12H are unzoned in CL, with medium brightness (Fig. 4a, analysis 2), and ca. 20% of the grains contain oscillatory zoned, bright, medium, or dark CL cores (Fig. 4a, analyses 5.1, 6, and 12). Ten analyses of the medium CL grains and rims yield 219-1109 ppm U, 1-6 ppm Th, Th/U = 0.003-0.010 (Table 1), and yield a concordia age of 431 ± 5 Ma (Fig. 4c; MSWD = 1.3, probability of equivalence = 0.15, probability of concordance = 0.245). Four additional analyses of medium CL grains yield 406-918 ppm U, 2-21 ppm Th, Th/U = 0.004-0.052, and yield variable younger and older ages that we interpret to reflect a combination of incomplete recrystallization of cores during metamorphism, slight analytical mixing with older cores, and minor Pb-loss (Fig. 4c, Table 1). Of a total of 21 trace element analyses, 6 contain elevated levels of contaminant elements (Fig. 4a, Table 2). The remaining REE patterns are characterized by flat HREE slopes (Yb_n/Gd_n = 1.5-5.2), and Eu anomalies are small (Eu/Eu* = 0.45-0.81; Fig. 4a, Table 2). Ti-in-zircon thermometry (Watson et al., 2006; Ferry and Watson, 2007) yields well-grouped results of 635-668 °C, with one outlier at 696 °C (Fig. 4d, Table 2). Electron microprobe and laser Raman analysis of the sparse inclusions identified garnet, phengite, rutile, quartz, graphite, and apatite.

Four analyses of oscillatory zoned cores reveal 129-509 ppm U, 29-220 ppm Th, Th/U = 0.23-0.68, and 1.92-2.43 Ga $^{207}Pb/^{206}Pb$ minimum ages (6-47% discordance; Table 1). Of five trace element analyses, two contain elevated levels of contaminant elements. The remaining REE patterns are characterized by steep HREE slopes (Yb_n/Gd_n = 6-15), and prominent negative Eu anomalies (Eu/Eu* = 0.08-0.31; Fig. 4a, Table 2). Ti-in-zircon thermometry (Watson et al., 2006; Ferry and Watson, 2007) yields 689-793 °C (Fig. 4d, Table 2). Electron microprobe and laser Raman analysis of the sparse inclusions identified quartz and apatite.

Garnet is nearly unzoned in major elements ($Alm_{80}Sps_2Prp_{12}Grs_6$, with a slight increase in Ca towards the rim) and trace elements (Eu/Eu* = 0.79-0.84, Yb_n/Gd_n = 2.2-3.5, with the exception of one outlier; Fig. 4b, Table 3). Two garnet inclusions in zircons analyzed by EMP ($Alm_{69}Sps_{12}Prp_8Grs_{11}$) are lower in Alm and Prp, and higher in Sps and Grs than garnet measured in thin section. Plagioclase is oligoclase (An_{11-19}). Muscovite contains a smaller phengite component than ZD21G (Si p.f.u. = 3.06-3.10). Three muscovite inclusions in zircons analyzed by EMP are higher in Si (Si p.f.u. = 3.18-3.21) than matrix muscovite analyzed in thin section.

6.3 Paragneiss ZD22A

Most zircons from paragneiss ZD22A contain oscillatory zoned, bright, medium, or dark CL cores surrounded by unzoned or weakly zoned medium to dark CL rims (Fig. 5a). Nine analyses of the medium CL rims and dark CL grains yield 239-805 ppm U, 4-110 ppm Th, Th/U = 0.007-0.21, and yield a range of ages between 391-795 Ma that we interpret to reflect a combination of incomplete recrystallization of cores during metamorphism, slight analytical mixing with older cores, and minor Pb-loss (Fig. 5b, Table 1). Seven analyses of oscillatory

zoned and dark CL cores reveal 28-787 ppm U, 13-525 ppm Th, Th/U = 0.20-2.39, and 1.35-2.55 Ga $^{207}Pb/^{206}Pb$ minimum ages (-3–140% discordance; Fig. 5b, Table 1). Of a total of 15 trace element analyses of both cores and rims, 6 contain elevated levels of contaminant elements (Fig. 5a, Table 2). The remaining REE patterns are characterized by steep HREE slopes (Yb_n/Gd_n = 8.4-151), and Eu anomalies are variable (Eu/Eu* = 0.15-1.04; one at 2.42 may reflect an unrecognized inclusion; Fig. 5a, Table 2). Ti-in-zircon thermometry (Watson et al., 2006; Ferry and Watson, 2007) yields scattered results of 600-789 °C (Fig. 5c; Table 2). Electron microprobe and laser Raman analysis of the sparse inclusions identified quartz, phengite, graphite, apatite, and one sphene inclusion.

7. Discussion

Mineral inclusions and REE patterns indicate that the 426 ± 4 Ma age of ZD21G and the 431 ± 5 Ma age of D12H, identical within error, reflect eclogite-facies zircon growth. The depletion in HREE indicates zircon growth in the presence of garnet, and the absence of negative Eu anomalies suggests that plagioclase was absent (Rubatto, 2002; Rubatto and Hermann, 2003; Schaltegger et al., 1999). Plagioclase in sample ZD21G contains a large positive Eu anomaly, but garnet and zircon lack the complementary negative Eu anomalies expected if these minerals were in trace element equilibrium (Fig. 3b, Table 3). We therefore interpret that the plagioclase in this sample is not in equilibrium with the garnet and zircon, and probably grew during exhumation and retrogression. Compositions of garnet and phengite inclusions in zircon from sample ZD21G are similar to compositions measured in thin section, consistent with concurrent growth of zircon, phengite, and garnet. In contrast, the compositions of garnet and phengite inclusions in zircon from sample D12H are different from compositions of matrix grains

measured in thin section. The inclusions of garnet contain higher Sps than observed in D12H thin section, possibly reflecting the composition of early-grown garnet no longer observed in thin section. The inclusions of phengite contain higher Si than observed in D12H thin section, and are compositionally similar to phengite cores in ZD21G. This may reflect more extensive retrograde recrystallization in sample D12H compared to ZD21G, and the ability of zircon to serve as a "container" that can preserve mineral compositions and assemblages that have been completely overprinted in the matrix (e.g., Katayama et al., 2002).

Results from Ti-in-zircon thermometry are tightly grouped at ~600 °C for sample ZD21G and ~660 °C for sample D12H. The presence of rutile and quartz inclusions in zircon indicates that assigning TiO_2 and SiO_2 activities = 1.0 is appropriate for these samples even though rutile is largely replaced by ilmenite in the groundmass. A complexity in interpreting the Ti-in-zircon thermometry is that the effect of pressure is not yet robustly calibrated. The values reported above are appropriate for pressures similar to the calibration conditions of P = 10 kbar, but a preliminary assessment of the pressure effect suggests that temperatures may be underestimated by as much as 50 °C for every increase in pressure of 10 kbar (Ferry and Watson, 2007). The apparent temperature difference between the two samples may indicate that pressure increased and/or temperature decreased during the time interval represented by these samples.

Preexisting zircon is commonly the most significant source of Zr for new zircon growth during metamorphism (Rubatto and Hermann, 2003). For the metasedimentary samples examined in this study, the preexisting zircon was of detrital origin, and eclogite facies metamorphism resulted in variable degrees of zircon growth and recrystallization in the three samples. Zircon in paragneiss ZD22A is dominated by the inherited component, and rims distinguished by CL imaging (e.g., Fig. 5a, analysis 1) show isotopic and trace element

inheritance. These data are consistent with solid-state recrystallization of detrital zircon with only minor new growth or dissolution/reprecipitation. In contrast, zircon in paragneiss ZD21G (and to a lesser extent D12H) is dominated by new metamorphic growth. Inherited cores are sparse, and the rims and metamorphic grains lack isotopic or trace element inheritance. Inclusions of metamorphic minerals (garnet, rutile, phengite) demonstrate that significant new metamorphic growth must have occurred, as solid-state recrystallization alone cannot account for the inclusions.

The least discordant inherited zircon core ages are 1.57-2.55 Ga, indicating that the protoliths of these rocks received sediments from Mesoproterozoic to Archean crust. Proterozoic to Archean zircon cores are also documented from several other localities in the North Qaidam terrane (Song et al., 2006; J.S. Yang et al., 2005; J.X. Zhang et al., 2008). The presence of this Proterozoic to Archean age component in inherited, detrital zircons argues against a Paleozoic to Mesozoic, subduction/accretion complex model of the Qaidam and adjacent Qilian terrane (Sengör and Natal'in, 1996). Half of the zircon core analyses group near 1.9 Ga and 2.5 Ga, similar to age probability peaks for the North China craton (Kusky and Li, 2003), possibly indicating a North China source for some of the sediments (Mattinson et al., 2007a). However, minor Paleoproterozoic to Archean rocks are also known from the Yangtze craton (Zheng et al., 2006), which also records 850-1000 Ma magmatism and metamorphism (Li et al., 2002), similar to ~900 Ma events in the North Qaidam terrane (Gehrels et al., 2003a, 2003b; Mattinson et al., 2006a, 2007b; J.X. Zhang et al., 2008). The North Qaidam terrane may therefore share a common Neoproterozoic history with the Yangtze craton (e.g., Song et al., 2006; Wan et al., 2006; J.X. Zhang et al., 2008).

The 426 ± 4 and 431 ± 5 Ma ages of eclogite-facies metamorphism are bracketed by previously reported ages of coesite-bearing zircon: the 423 ± 6 Ma weighted mean age of coesite-bearing paragneiss (Song et al., 2006), and the 427 ± 4 Ma, 439 ± 3 Ma, and 440 ± 17 Ma ages of individual SHRIMP analyses from two other samples (J.S. Yang et al., 2005). Raman analysis of our samples reveals inclusions of quartz, but no coesite. However, only one quartz inclusion was identified in a dated zircon rim (D12H-3). The scarcity of coesite inclusions documented in previous studies (Song et al., 2003a, 2003b, 2006; J.S. Yang et al., 2001a, 2005) indicates that the number of zircons investigated in this study (ca. 400 grains) may have been too few to reveal the presence of coesite.

The age range of 459-422 Ma interpreted to reflect HP/UHP conditions in eclogite from the Dulan area (Mattinson et al., 2006b; Song et al., 2003a, 2006; G. Zhang et al., 2008) overlaps the 440-423 Ma age range for coesite-bearing zircon from paragneiss (Song et al., 2006; J.S. Yang et al., 2005), but extends to older ages. Further work is required to determine if the range of ages reflects protracted residence at eclogite-facies conditions (Mattinson et al., 2006b; McClelland et al., 2006; Lapen et al., 2003) or is the result of multiple HP/UHP events resulting from complex P-T-t paths (Song et al., 2006; Stöckhert and Gerya, 2005). In either case, the youngest UHP metamorphism at 423 Ma was followed by exhumation, amphibolite-facies overprinting resulting in the growth of plagioclase and ilmenite in the paragneiss, and cooling below the muscovite Ar closure temperature by 402 ± 2 Ma (Song et al., 2006). This study illustrates the paragenetic complexities of eclogite facies zircon growth in paragneisses of close proximity.

Acknowledgements

We thank C.L. Wu, A. Bian, and S.Y. Chen for assistance in the field, B. Ito and F.K. Mazdab for assistance with the development of the SHRIMP-RG trace element analysis technique, B. Wiegand, U. Martens, and A. Strickland for assistance with the SHRIMP-RG analyses, B. Jones for assistance with the EMP analyses, L. Heister for assistance with the LA-ICPMS analyses, and L. Yan for assistance with the laser Raman analyses. The manuscript was improved by suggestions from associate editor S. Song and two anonymous reviewers. This research was supported by grants from Stanford University, the Geological Society of America (Grant #7466-03), and the National Science Foundation (NSF-EAR0408690 and NSF-EAR0710927).

References

Black, L.P., Kamo, S.L., Allen, C.M., Davis, D.W., Aleinikoff, J.N., Valley, J.W., Mundil, R., Campbell, I.H., Korsch, R.J., Williams, I.S. and Foudoulis, C., 2004. Improved $^{206}Pb/^{238}U$ microprobe geochronology by the monitoring of a trace-element-related matrix effect; SHRIMP, ID-TIMS, ELA-ICP-MS and oxygen isotope documentation for a series of zircon standards. Chemical Geology 205, 115-140.

Brueckner, H.K. and Van Roermund, H.L.M., 2004. Dunk tectonics: A multiple subduction/eduction model for the evolution of the Scandinavian Caledonides. Tectonics 23, TC2004, doi:10.1029/2003TC001502.

Chopin, C., 2003. Ultrahigh-pressure metamorphism: tracing continental crust into the mantle. Earth and Planetary Science Letters 212, 1-14.

Coleman, R.G. and Wang, X., 1995. Overview of the geology and tectonics of UHPM. In: R.G. Coleman and X. Wang (Eds.), Ultrahigh Pressure Metamorphism. Cambridge University Press, New York, pp. 1-32.

Coryell, C.D., Chase, J.W. and Winchester, J.W., 1963. A procedure for geochemical interpretation of terrestrial rare-earth abundance patterns. Journal of Geophysical Research 68, 559-566.

Ferry, J. and Watson, E., 2007. New thermodynamic models and revised calibrations for the Ti-in-zircon and Zr-in-rutile thermometers. Contributions to Mineralogy and Petrology 154, 429-437.

Gehrels, G.E., Yin, A. and Wang, X.-F., 2003a. Detrital-zircon geochronology of the northeastern Tibetan plateau. Geological Society of America Bulletin 115, 881-896.

Gehrels, G.E., Yin, A. and Wang, X.-F., 2003b. Magmatic history of the northeastern Tibetan Plateau. Journal of Geophysical Research 108, 2423, doi:10.1029/2002JB001876.

Hacker, B., 2007. Ascent of the ultrahigh-pressure Western Gneiss Region, Norway. In: M. Cloos, W.D. Carlson, M.C. Gilbert, J.G. Liou and S.S. Sorenson (Eds.), Geological Society of America Special Paper 419, Convergent Margin Terranes and Associated Regions: A Tribute to W.G. Ernst, pp. 171-184.

Katayama, I., Ohta, M. and Ogasawara, Y., 2002. Mineral inclusions in zircon from diamond-bearing marble in the Kokchetav massif, northern Kazakhstan. European Journal of Mineralogy 14, 1103-1108.

Kusky, T.M. and Li, J., 2003. Paleoproterozoic tectonic evolution of the North China Craton. Journal of Asian Earth Sciences 22, 383-397.

Kylander-Clark, A.R.C., Hacker, B.R., Johnson, C.M., Beard, B.L., Mahlen, N.J. and Lapen, T.J., 2007. Coupled Lu-Hf and Sm-Nd geochronology constrains prograde and exhumation histories of high- and ultrahigh-pressure eclogites from western Norway. Chemical Geology 242, 137-154.

Lapen, T.J., Johnson, C.M., Baumgartner, L.P., Mahlen, N.J., Beard, B.L. and Amato, J.M., 2003. Burial rates during prograde metamorphism of an ultra-high-pressure terrane: an example from Lago di Cignana, western Alps, Italy. Earth and Planetary Science Letters 215, 57-72.

Li, Z.-X., Li, X.-h., Zhou, H. and Kinny, P.D., 2002. Grenvillian continental collision in south China: New SHRIMP U-Pb zircon results and implications for the configuration of Rodinia. Geology 30, 163-166.

Liati, A., 2005. Identification of repeated Alpine (ultra) high-pressure metamorphic events by U-Pb SHRIMP geochronology and REE geochemistry of zircon: the Rhodope zone of Northern Greece. Contributions to Mineralogy and Petrology 150, 608-630.

Liou, J.G., Liou, J. G., Ernst, W. G., Zhang, R. Y., Tsujimori, T., and Jahn, B. M., in press, Ultrahigh-P minerals and metamorphic terranes–a perspective view: Journal of Asian Earth Sciences.

Liu, L., Sun, Y., Xiao, P., Che, Z., Luo, J., Chen, D., Wang, Y., Zhang, A., Chen, L. and Wang, Y., 2002. Discovery of ultrahigh-pressure magnesite-bearing garnet lherzolite (>3.8 GPa) in the Altyn Tagh, Northwest China. Chinese Science Bulletin 47, 881-886.

Lu, S.-n., Wang, H.-c., Li, H.-k., Yuan, G.-b., Xin, H.-t., and Zheng, J.-k., 2002, Redefinition of the “Dakendaban Group” on the northern margin of the Qaidam basin: Geological Bulletin of China, v. 21, no. 1, p. 19-23 (in Chinese with English abstract).

Ludwig, K.R., 1998. On the treatment of concordant uranium-lead ages. Geochimica et Cosmochimica Acta 62, 665-676.

Ludwig, K.R., 2001. Squid 1.02: A user's manual. Berkeley Geochronology Center Special Publication No. 2, Berkeley, U.S.A., 19 pp.

Ludwig, K.R., 2003. User's manual for Isoplot 3.00: A geochronological toolkit for Microsoft Excel. Berkeley Geochronology Center Special Publication No. 4, Berkeley, U.S.A., 70 pp.

Maas, R., Kinny, P.D., Williams, I.S., Froude, D.O. and Compston, W., 1992. The Earth's oldest known crust: A geochronological and geochemical study of 3900--4200 Ma detrital zircons from Mt. Narryer and Jack Hills, Western Australia. Geochimica et Cosmochimica Acta 56, 1281-1300.

Mattinson, C.G., Menold, C.A., Zhang, J.X. and Bird, D.K., 2007a. High- and Ultrahigh-Pressure Metamorphism in the North Qaidam and South Altyn Terranes, Western China. International Geology Review 49, 969-995.

Mattinson, C.G., Tsujimori, T., Zhang, R.Y. and Liou, J.G., 2004. Epidote-rich talc-kyanite-phengite eclogites, Sulu terrane, eastern China: P-T-fO_2 estimates and the significance of the epidote-talc assemblage in eclogite. American Mineralogist 89, 1772-1783.

Mattinson, C.G., Wooden, J.L., Liou, J.G., Bird, D.K. and Wu, C.L., 2006a. Geochronology and tectonic significance of Middle Proterozoic granitic orthogneiss, North Qaidam HP/UHP terrane, Western China. Mineralogy and Petrology 88, 227-241.

Mattinson, C.G., Wooden, J.L., Liou, J.G., Bird, D.K. and Wu, C.L., 2006b. Age and duration of eclogite-facies metamorphism, North Qaidam HP/UHP terrane, western China. American Journal of Science 306, 683-711.

Mattinson, C.G., Wooden, J.L., Mazdab, F.K., Zhang, J., Bird, D.K. and Liou, J.G., 2007b. Monazite and zircon record Proterozoic and Paleozoic metamorphism of paragneiss, North Qaidam UHP terrane, NW China. Eos Transactions, AGU 88, Fall meeting supplement, Abstract V41C-0711.

Mazdab, F.K. and Wooden, J.L., 2006. Trace element analysis in zircon by ion microprobe (SHRIMP-RG): Technique and applications. Geochimica et Cosmochimica Acta 70, 26-26.

Mazdab, F.K. and Wooden, J.L., in review. Trace element analysis in zircon by ion microprobe (SHRIMP-RG): Technique and applications. U.S. Geological Survey Open-File Report.

McClelland, W.C., Power, S.E., Gilotti, J.A., Mazdab, F.K. and Wopenka, B., 2006. U-Pb SHRIMP geochronology and trace element geochemistry of coesite-bearing zircons, North-East Greenland Caledonides. In: B.R. Hacker, B. McClelland and J.G. Liou (Eds.), Geological Society of America Special Paper 403, Ultrahigh-Pressure Metamorphism: Deep Continental Subduction. Geological Society of America, pp. 23-43.

McDonough, W.F. and Sun, S.-s., 1995. The composition of the Earth. Chemical Geology 120, 223-253.

Menold, C. A., Manning, C. E., Yin, A., Chen, X.-H., and Wang, X.-F., in review, Metamorphic evolution, mineral chemistry and thermobarometry of ultrahigh-pressure eclogites from the North Qaidam metamorphic belt, Western China: Journal of Metamorphic Geology.

Pearce, N.J.G., Perkins, W.T., Westgate, J.A., Gorton, M.P., Jackson, S.E., Neal, C.R. and Chenery, S.P., 1997. A compilation of new and published major and trace element data for NIST SRM 610 and NIST SRM 612 glass reference materials. Geostandards Newsletter 21, 115-144.

Ratschbacher, L., Hacker, B.R., Calvert, A., Webb, L.E., Grimmer, J.C., McWilliams, M.O., Ireland, T., Dong, S. and Hu, J., 2003. Tectonics of the Qinling (Central China): tectonostratigraphy, geochronology, and deformation history. Tectonophysics 366, 1-53.

Rubatto, D., 2002. Zircon trace element geochemistry: partitioning with garnet and the link between U-Pb ages and metamorphism. Chemical Geology 184, 123-138.

Rubatto, D. and Hermann, J., 2003. Zircon formation during fluid circulation in eclogites (Monviso, Western Alps): Implications for Zr and Hf budget in subduction zones. Geochimica et Cosmochimica Acta 67, 2173-2187.

Rubatto, D. and Scambelluri, M., 2003. U-Pb dating of magmatic zircon and metamorphic baddeleyite in the Ligurian eclogites (Voltri Massif, Western Alps). Contributions to Mineralogy and Petrology 146, 341-355.

Schaltegger, U., Fanning, C.M., Günther, D., Maurin, J.C., Schulmann, K. and Gebauer, D., 1999. Growth, annealing and recrystallization of zircon and preservation of monazite in high-grade metamorphism: conventional and in-situ U-Pb isotope, cathodoluminescence and microchemical evidence. Contributions to Mineralogy and Petrology 134, 186-201.

Sengör, A.M.C. and Natal'in, B.A., 1996. Paleotectonics of Asia: fragments of a synthesis. In: A. Yin and M. Harrison (Eds.), The Tectonic Evolution of Asia. Cambridge University Press, New York, pp. 486-640.

Song, S., Yang, J., Liou, J.G., Wu, C., Shi, R. and Xu, Z., 2003a. Petrology, geochemistry and isotopic ages of eclogites from the Dulan UHPM terrane, the North Qaidam, NW China. Lithos 70, 195-211.

Song, S., Zhang, L., Niu, Y., Li, S., Song, B. and Liu, D., 2006. Evolution from oceanic subduction to continental collision: a case study from the northern Tibetan Plateau based on geochemical and geochronological data. Journal of Petrology 47, 435-455.

Song, S., Zhang, L., Niu, Y., Su, L., Jian, P. and Liu, D., 2005. Geochronology of diamond-bearing zircons from garnet peridotite in the North Qaidam UHPM belt, Northern Tibetan

Plateau: A record of complex histories from oceanic lithosphere subduction to continental collision. Earth and Planetary Science Letters 234, 99-118.

Song, S.G., Yang, J.S., Xu, Z.Q., Liou, J.G. and Shi, R.D., 2003b. Metamorphic evolution of the coesite-bearing ultrahigh-pressure terrane in the North Qaidam, Northern Tibet, NW China. Journal of Metamorphic Geology 21, 631-644.

Stöckhert, B. and Gerya, T.V., 2005. Pre-collisional high pressure metamorphism and nappe tectonics at active continental margins: a numerical simulation. Terra Nova 17, 102-110.

Stacey, J.S. and Kramers, J.D., 1975. Approximation of terrestrial lead isotope evolution by a two-stage model. Earth and Planetary Science Letters 26, 207-221.

Steiger, R.H. and Jäger, E., 1977. Subcommission on geochronology: Convention on the use of decay constants in geo- and cosmochemistry. Earth and Planetary Science Letters 36, 359-362.

Wan, Y., Li, R., Wilde, S.A., Liu, D., Chen, Z., Yan, L., Song, T. and Yin, X., 2005. UHP metamorphism and exhumation of the Dabie Orogen, China: Evidence from SHRIMP dating of zircon and monazite from a UHP granitic gneiss cobble from the Hefei Basin. Geochimica et Cosmochimica Acta 69, 4333-4348.

Wan, Y., Zhang, J., Yang, J. and Xu, Z., 2006. Geochemistry of high-grade metamorphic rocks of the North Qaidam mountains and their geological significance. Journal of Asian Earth Sciences 28, 174-184.

Wan, Y.S., Xu, Z.Q., Yang, J.S. and Zhang, J.X., 2001. Ages and compositions of the Precambrian high-grade basement of the Qilian Terrane and its adjacent areas. Acta Geologica Sinica 75, 375-384.

Watson, E., Wark, D. and Thomas, J., 2006. Crystallization thermometers for zircon and rutile. Contributions to Mineralogy and Petrology 151, 413-433.

Williams, I.S., 1998. U-Th-Pb geochronology by ion microprobe. In: M.A. McKibben, W.C. Shanks, III and W.I. Ridley (Eds.), Reviews in Economic Geology Vol. 7: Applications of microanalytical techniques to understanding mineralizing processes. Society of Economic Geologists, pp. 1-35.

Wu, C., Yang, J., Wooden, J., Ernst, W.G., Liou, J.G., Li, H., Zhang, J., Wan, Y. and Shi, R., 2001. Relationship between UHP eclogite and two different types of granite in the North Qaidam, NW China: Evidence from zircon SHRIMP ages of granites. Eos Transactions, AGU 82, Abstract V32C-0980.

Wu, C., Yang, J., Wooden, J.L., Shi, R., Chen, S., Meibom, A. and Mattinson, C., 2004. Zircon U-Pb SHRIMP dating of the Yematan Batholith in Dulan, north Qaidam, NW China. Chinese Science Bulletin 49, 1736-1740.

Yang, J.J. and Deng, J.F., 1994. Garnet peridotites and eclogites in the northern Qaidam Mountains, Tibetan plateau: a first record, First Workshop on UHP Metamorphism and Tectonics. ILP Task Group III-6, Stanford University, pp. A-20.

Yang, J.S., Liu, F., Wu, C., Xu, Z., Shi, R. and Chen, S., 2005. Two ultrahigh-pressure metamorphic events recognized in the Central Orogenic Belt of China: Evidence from the U-Pb dating of coesite-bearing zircons. International Geology Review 47, 327-343.

Yang, J.S., Xu, Z., Song, S., Wu, C., Shi, R., Zhang, J., Wan, Y., Li, H., Jin, X. and Jolivet, M., 2000. Discovery of eclogite in Dulan, Qinghai Province and its significance for studying the HP--UHP metamorphic belt along the Central Orogenic Belt of China. Acta Geologica Sinica 74, 156-168 (in Chinese with English abstract).

Yang, J.S., Xu, Z., Song, S., Zhang, J., Wu, C., Shi, R., Li, H., and Brunel, M., 2001a, Discovery of coesite in the North Qaidam Early Palaeozoic ultrahigh pressure (UHP) metamorphic belt, NW China: Earth and Planetary Sciences, v. 333, p. 719-724.

Yang, J.S., Xu, Z., Zhang, J., Chu, C.-Y., Zhang, R. and Liou, J.-G., 2001b. Tectonic significance of Early Paleozoic high-pressure rocks in Altun--Qaidam--Qilian Mountains, NW China. Geological Society of America Memoir 194, 151-170.

Yang, J.S., Xu, Z., Zhang, J., Song, S., Wu, C., Shi, R., Li, H. and Brunel, M., 2002. Early Paleozoic North Qaidam UHP metamorphic belt on the north-eastern Tibetan plateau and a paired subduction model. Terra Nova 14, 397-404.

Yin, A. and Harrison, T.M., 2000. Geologic evolution of the Himalayan-Tibetan orogen. Annual Review of Earth and Planetary Sciences 28, 211-280.

Yin, A., Manning, C.E., Lovera, O., Menold, C.A., Chen, X. and Gehrels, G.E., 2007. Early Paleozoic Tectonic and Thermomechanical Evolution of Ultrahigh-Pressure (UHP) Metamorphic Rocks in the Northern Tibetan Plateau, Northwest China. International Geology Review 49, 681-716.

Zhang, G., Song, S., Zhang, L. and Niu, Y., 2008. The subducted oceanic crust within continental-type UHP metamorphic belt in the North Qaidam, NW China: Evidence from petrology, geochemistry and geochronology. Lithos 104, 99-118.

Zhang, J., Mattinson, C.G., Meng, F., Wan, Y. and Dong, K., 2008. Polyphase tectonothermal history recorded in granulitized gneisses from the North Qaidam HP/UHP metamorphic terrane, Western China: evidence from zircon U-Pb geochronology. Geological Society of America Bulletin 120, 732-749.

Zhang, J.X., Mattinson, C.G., Meng, F.C. and Wan, Y.S., 2005a. An Early Palaeozoic HP/HT granulite-garnet peridotite association in the south Altyn Tagh, NW China: P-T history and U-Pb geochronology. Journal of Metamorphic Geology 23, 491-510.

Zhang, J.X., Yang, J.S., Mattinson, C.G., Xu, Z.Q., Meng, F.C. and Shi, R.D., 2005b. Two contrasting eclogite cooling histories, North Qaidam HP/UHP terrane, western China: Petrological and isotopic constraints. Lithos 84, 51-76.

Zheng, J., Griffin, W.L., O'Reilly, S.Y., Zhang, M., Pearson, N. and Pan, Y., 2006. Widespread Archean basement beneath the Yangtze craton. Geology 34, 417-420.

Figure captions

Fig. 1. (a) Map of China showing the location of this study (box) and the trends of major mountain belts (dashed lines). NCC, North China craton; YC, Yangtze craton. (b) Schematic map of the Qaidam-Qilian-Altyn Tagh region showing major tectonic units, and locations of eclogite and garnet peridotite. The box near Dulan (lower right corner) indicates the location of Fig. 2. Modified from J.X. Zhang et al. (2005a) and Mattinson et al. (2007a).

Fig. 2. Geologic sketch map of the study area showing sample locations. Foliation in the Dakendaban Group is dominantly northwest striking, steeply northeast dipping, locally modified by tight, northwest plunging folds. Granite and granodiorite are part of the Yematan batholith (397 ± 3 Ma; Wu et al., 2004). The town of Dulan is approximately 30 km southwest of map area. Modified from Mattinson et al. (2007a) and J.S. Yang et al. (2000).

Fig. 3. (a) Cathodoluminescence (CL) images and REE patterns for paragneiss ZD21G zircon. REE patterns marked by unfilled circles represent medium or dark CL zircon, filled squares represent cores, and grey lines without symbols represent analyses with elevated levels of contaminant elements (see text). Circles on CL images show the locations of ~30μm SHRIMP-RG analyses, labeled with their analysis number (Tables 1 and 2) and ^{207}Pb-corrected ^{206}Pb/^{238}U age and 1σ error (^{204}Pb-corrected ^{207}Pb/^{206}Pb for ages >1 Ga; no age for trace element-only analyses). (b) REE patterns for paragneiss ZD21G garnet (unfilled circles) and plagioclase (filled squares). (c) Tera-Wasserburg concordia diagram for paragneiss ZD21G zircon (cores not plotted). Filled circles indicate analyses included in the concordia age. Plotted ratios are uncorrected for common-Pb, and error ellipses are 2σ. (d) Histogram and relative probability plot for paragneiss ZD21G Ti-in-zircon thermometry (±10 °C uncertainty assigned to each analysis; Watson et al., 2006).

Fig. 4. (a) Cathodoluminescence (CL) images and REE patterns for paragneiss D12H zircon. REE patterns marked by unfilled circles represent medium or dark CL zircon, filled squares represent cores, and grey lines without symbols represent analyses with elevated levels of contaminant elements (see text). Circles in CL images show the locations of ~30μm SHRIMP-RG analyses, labeled with their analysis number (Tables 1 and 2) and ^{207}Pb-corrected ^{206}Pb/^{238}U age and 1σ error (^{204}Pb-corrected ^{207}Pb/^{206}Pb for ages >1 Ga). (b) REE patterns for paragneiss D12H garnet. (c) Tera-Wasserburg concordia diagram for paragneiss D12H zircon (cores not plotted). Filled circles indicate analyses included in the concordia age. Plotted ratios are uncorrected for common-Pb, and error ellipses are 2σ. (d) Histogram and relative probability

plot for paragneiss D12H Ti-in-zircon thermometry (±10 °C uncertainty assigned to each analysis; Watson et al., 2006).

Fig. 5. (a) Cathodoluminescence (CL) images and REE patterns for paragneiss ZD22A zircon. REE patterns marked by unfilled circles represent rims, filled squares represent cores, and grey lines without symbols represent analyses with elevated levels of contaminant elements (see text). Circles in CL images show the locations of ~30μm SHRIMP-RG analyses, labeled with their analysis number (Tables 1 and 2) and ^{207}Pb-corrected ^{206}Pb/^{238}U age and 1σ error (^{204}Pb-corrected ^{207}Pb/^{206}Pb for ages >1 Ga; no age for trace element-only analyses). (b) Wetherill concordia diagram for paragneiss ZD22A zircon showing all analyses. Plotted ratios are ^{204}Pb-corrected for common-Pb, and error ellipses are 2σ. (c) Histogram and relative probability plot for paragneiss ZD22A Ti-in-zircon thermometry (±10 °C uncertainty assigned to each analysis; Watson et al., 2006).

Figure 1

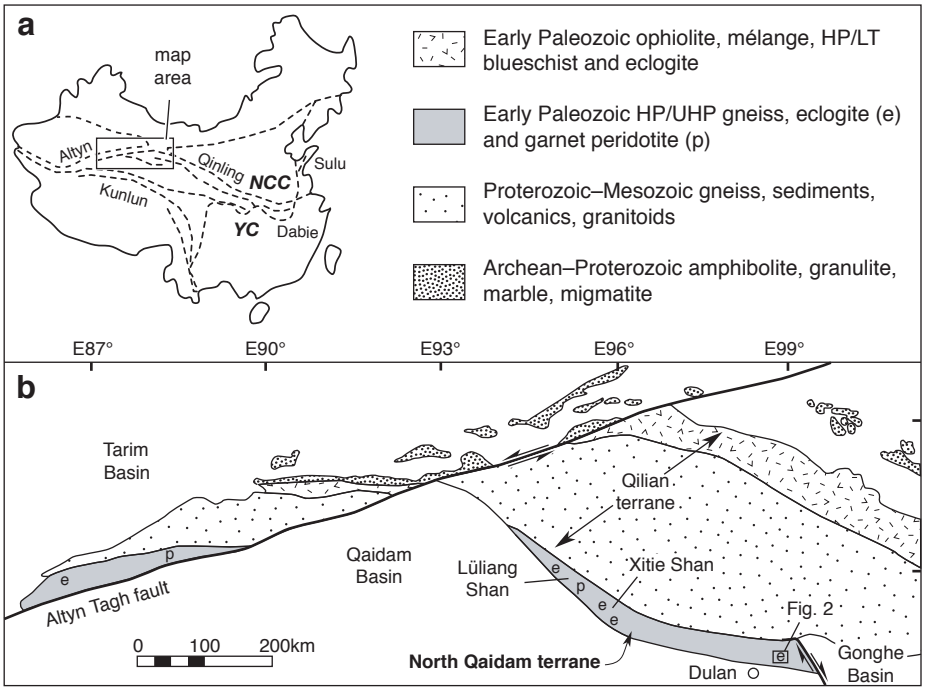

Fig. 1

Figure 2

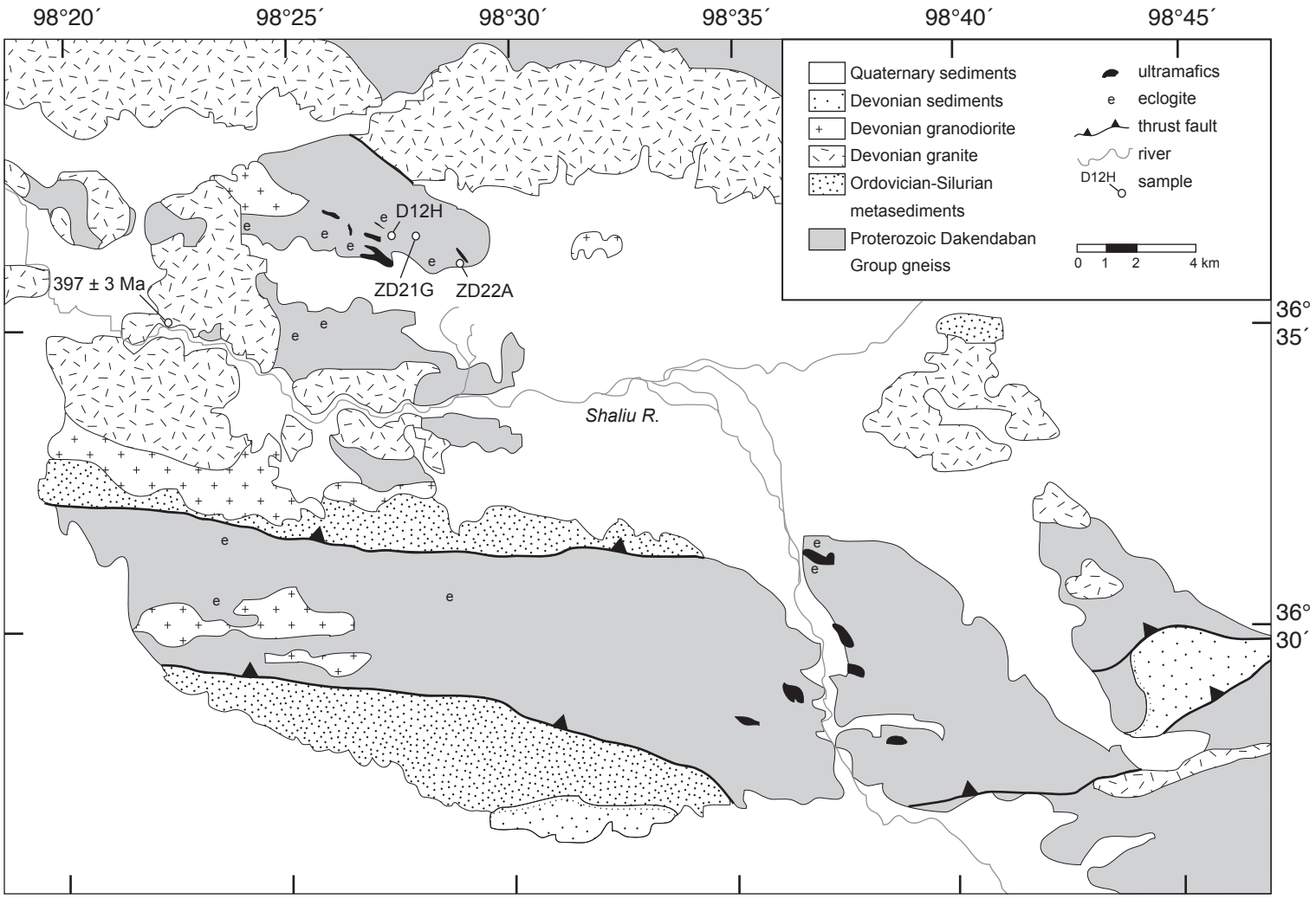

Fig. 2

Figure 3

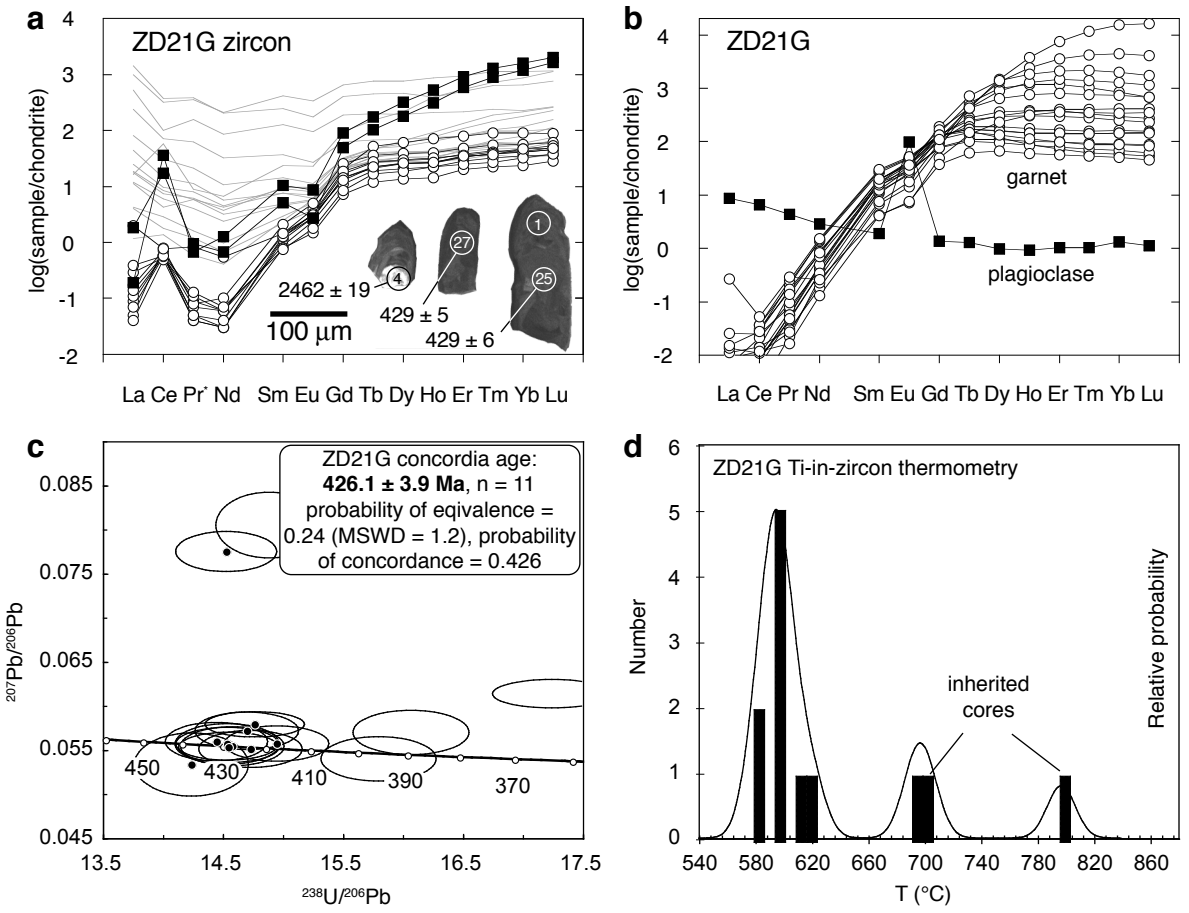

Fig. 3

Figure 4

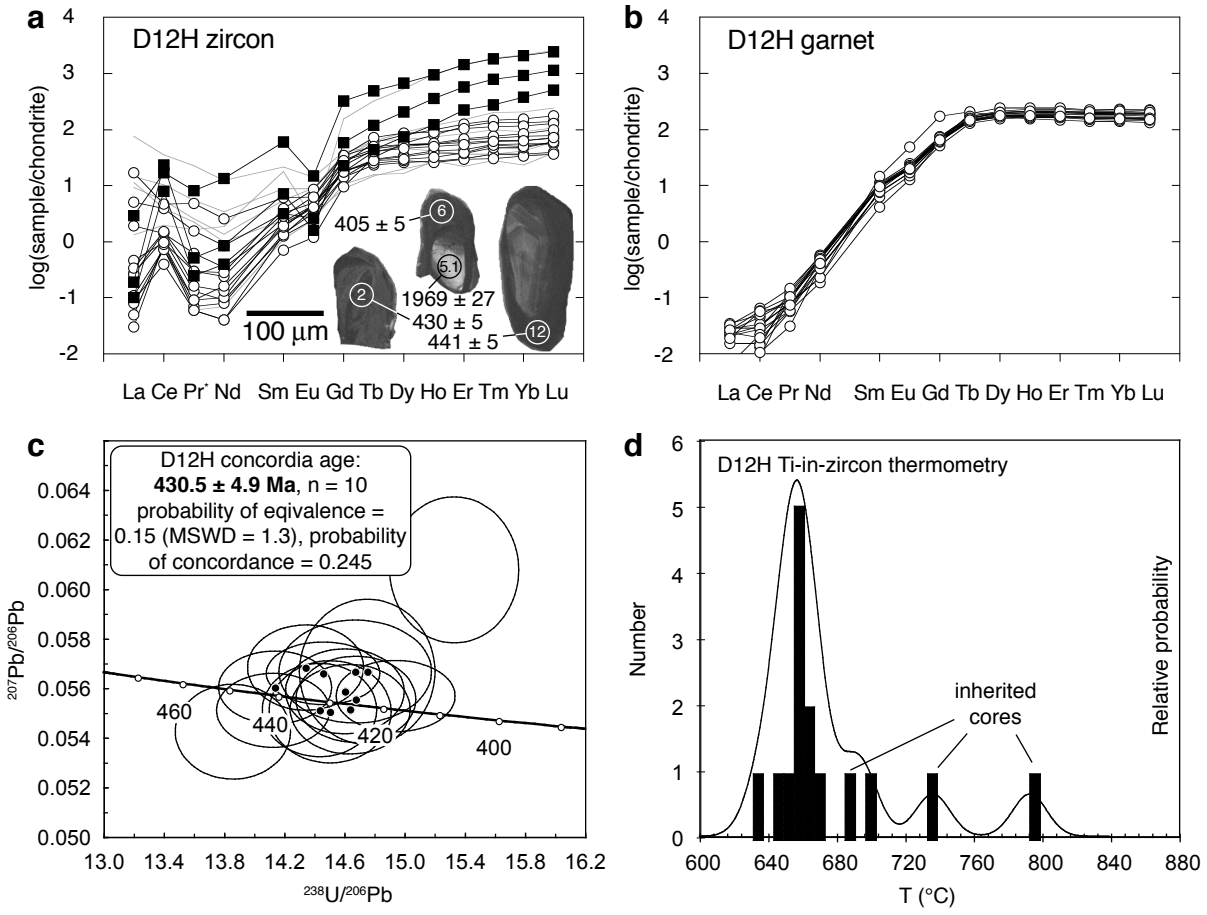

Fig. 4

Figure 5

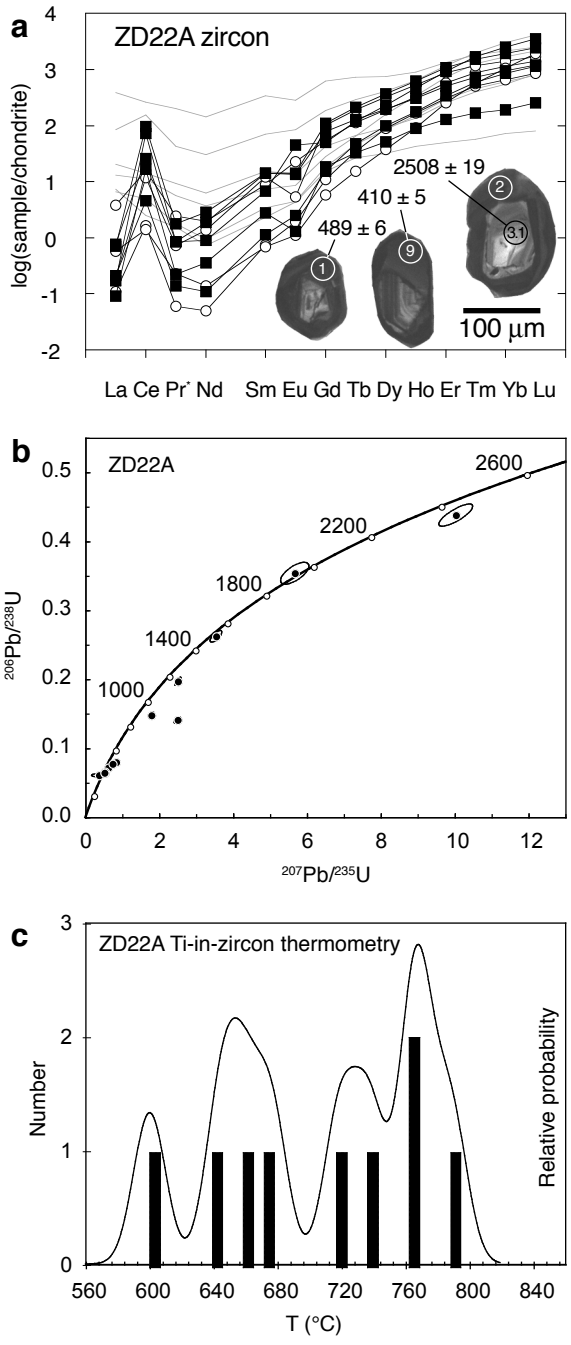

Fig. 5

Table 1

Table 1: Zircon U-Pb isotopic data, paragneiss samples D12H, ZD21G, and ZD22A, North Qaidam terrane, western China.

analysis	CL	$^{206}Pb_c$ (%)	ppm U	ppm Th	$^{232}Th/^{238}U$	^{207}Pb-corr $^{206}Pb/^{238}U$ Age (Ma)	1σ err	$^{207}Pb/^{206}Pb$ Age (Ma)	1σ err	% Disc.	Total $^{238}U/^{206}Pb$	% err	Total $^{207}Pb/^{206}Pb$	% err
D12H-1*	r	0.16	571	4	0.007	433.9	± 4.7				14.34	1.1	.0569	1.2
D12H-2*	m	--	396	3	0.007	430.1	± 4.8				14.50	1.1	.0551	1.5
D12H-3*	d	--	570	4	0.007	426.2	± 4.7				14.63	1.1	.0552	1.3
D12H-04*	m	0.18	219	1	0.005	422.2	± 5.2				14.75	1.2	.0567	2.1
D12H-05*	m	0.17	691	2	0.003	424.4	± 5.9				14.67	1.4	.0567	1.5
D12H-06	m	0.74	406	21	0.052	404.5	± 4.6				15.33	1.1	.0608	2.0
D12H-07*	m	0.03	607	6	0.010	424.9	± 4.6				14.67	1.1	.0556	1.3
D12H-08*	r	0.04	801	4	0.006	440.5	± 4.7				14.14	1.1	.0561	1.1
D12H-010*	d	--	979	5	0.005	432.1	± 4.6				14.43	1.1	.0551	1.4
D12H-011*	m	0.07	615	3	0.005	426.8	± 4.6				14.60	1.1	.0559	1.3
D12H-012	r	--	777	4	0.006	441.4	± 4.7				14.12	1.1	.0551	1.1
D12H-16*	d	0.14	1109	3	0.003	430.6	± 4.5				14.45	1.1	.0566	0.9
D12H-17	r	0.07	918	5	0.006	417.5	± 4.4				14.94	1.1	.0557	1.1
D12H-18	m	--	492	2	0.004	450.1	± 5.0				13.86	1.1	.0543	1.4
D12H-8.1	oc	6.89	332	220	0.685	1519.5	± 16.4	2376	± 14	47	3.50	0.7	.1537	0.7
D12H-5.1	bc	3.31	129	29	0.230	1535.2	± 20.9	1969	± 27	25	3.60	1.3	.1238	1.1
D12H-14.1	oc	0.92	509	191	0.388	1789.4	± 20.6	1916	± 10	6	3.10	1.2	.1174	0.5
D12H-15.1	oc	1.85	455	166	0.378	2239.4	± 27.3	2425	± 8	7	2.36	1.2	.1574	0.4
ZD21G-6	dc	0.96	1174	18	0.016	360.2	± 4.2				17.24	1.2	.0615	1.1
ZD21G-8	m	0.33	442	1	0.003	388.1	± 4.7				16.06	1.2	.0571	1.8
ZD21G-9*	d	0.34	1177	5	0.005	421.2	± 4.7				14.76	1.1	.0580	1.0
ZD21G-12*	m	0.08	580	4	0.007	417.2	± 4.9				14.94	1.2	.0558	1.5
ZD21G-13	d	--	362	1	0.004	396.1	± 4.8				15.79	1.2	.0541	1.9
ZD21G-16*	d	0.07	500	2	0.004	431.3	± 5.1				14.44	1.2	.0560	1.6
ZD21G-17*	d	0.04	702	5	0.007	428.9	± 5.1				14.53	1.2	.0558	1.4
ZD21G-18	d	6.02	1586	77	0.050	377.7	± 5.2				15.58	1.1	.1027	0.7
ZD21G-19	c	1.27	152	86	0.582	1003.9	± 12.9	1265	± 31	25	5.86	1.3	.0833	1.6
ZD21G-20	d	3.18	469	3	0.006	406.4	± 5.2				14.88	1.2	.0806	1.9
ZD21G-21*	m	--	189	1	0.006	438.9	± 5.9				14.23	1.4	.0534	2.7
ZD21G-22*	d	--	541	2	0.004	423.6	± 5.0				14.73	1.2	.0552	1.6
ZD21G-23*	m	0.01	491	2	0.003	427.8	± 5.1				14.57	1.2	.0555	1.6
ZD21G-24*	m	2.77	624	15	0.025	417.7	± 5.1				14.52	1.2	.0776	1.2
ZD21G-25*	m	0.04	450	1	0.003	428.9	± 5.1				14.53	1.2	.0558	1.7
ZD21G-26*	m	0.24	544	8	0.016	423.4	± 5.0				14.69	1.2	.0572	1.5
ZD21G-27*	m	--	787	3	0.004	428.7	± 4.9				14.54	1.2	.0554	1.3
ZD21G-4	bc	5.79	68	64	0.975	1823.6	± 21.3	2462	± 19	28	2.88	0.9	.1619	1.1
ZD21G-15	oc	1.63	532	198	0.385	654.3	± 3.0	1025	± 36	54	9.21	0.4	.0748	1.6
ZD22A-01	r	2.20	627	35	0.058	488.7	± 5.9	1030	± 29	107	12.42	1.2	.0748	1.4
ZD22A-02	dc	1.74	787	525	0.688	1147.3	± 12.9	1452	± 14	25	5.04	1.1	.0927	0.6
ZD22A-3	oc	2.28	68	56	0.848	2300.9	± 36.6	2514	± 19	7	2.28	1.5	.1663	1.1
ZD22A-03	r	0.76	516	28	0.056	449.3	± 5.3	605	± 45	34	13.75	1.2	.0620	1.5
ZD22A-04	dc	2.16	608	145	0.247	874.4	± 10.3	1350	± 16	51	6.73	1.2	.0861	0.8
ZD22A-05	r	2.85	239	5	0.021	391.4	± 5.9				15.52	1.3	.0775	7.0
ZD22A-06	d	1.31	805	38	0.049	479.2	± 5.5	841	± 23	73	12.79	1.2	.0673	1.1
ZD22A-07	oc	0.45	137	168	1.261	1500.0	± 19.2	1570	± 23	4	3.80	1.3	.0974	1.2
ZD22A-08	d	0.36	589	6	0.010	405.2	± 4.8				15.36	1.2	.0577	2.3
ZD22A-09	r	0.33	620	8	0.014	409.6	± 4.8				15.19	1.2	.0576	1.4
ZD22A-010	r	0.17	530	4	0.007	416.0	± 4.9				14.98	1.2	.0564	1.5
ZD22A-011	d	7.33	554	110	0.205	795.1	± 11.6	2055	± 12	140	7.06	1.2	.1262	0.7
ZD22A-012	m	0.07	285	4	0.014	407.8	± 5.1				15.30	1.3	.0555	2.1
ZD22A-013	bc	--	28	65	2.386	1965.2	± 35.9	1891	± 37	-3	2.82	1.8	.1160	2.1
ZD22A-1	oc	2.60	205	190	0.958	2257.9	± 15.2	2513	± 9	9	2.32	0.6	.1656	0.6
ZD22A-7	bc	4.70	32	13	0.399	2067.6	± 31.3	2549	± 27	18	2.52	1.4	.1691	1.6

Note: Analyses performed 3-4 March 2005, for which the error in standard calibration was 0.66% (2σ), except D12H-1-18 (23-24 June 2006; 1.01%), and D12H-8.1, ZD21G-4, 15, ZD22A-1, 7 (10-11 October 2003; 0.44%). The error in standard calibration is not included in the errors above, but is required when comparing data from different sessions. Samples marked with asterisks are included in the concordia ages. Abbreviations of CL textures: c, medium CL core; d, dark CL grain; m, medium CL grain; r, medium CL rim; bc, bright CL core; dc, dark CL core; dr, dark CL rim; oc, oscillatory zoned core.

Table 2

Table 2: Zircon trace element data, paragneiss samples D12H, ZD21G, and ZD22A, North Qaidam terrane, western China. Concentrations in ppm except as noted. Samples in italics contain elevated levels of contaminant elements (see text). Ti-in-zircon thermometry calibration from Watson et al. (2006).

analysis	CL	Be	B	F	Al	P	S	Cl	Ca	Sc	Ti	Ti	V	Mn	Fe	Ge	Y	Nb	Zr94H
					Rel.		Rel.	Rel.	Rel.		(^{48}Ti)	(^{49}Ti)	Rel.	Rel.					Rel.
D12H-2	m	0.19	1.36	18	2	149	1	0	4	86.8	4.3	4.2	1.2	2	5	0.2	154	1.3	5.5
D12H-3	d	0.19	0.38	16	1	78	1	1	3	73.7	6.1	6.3	0.2	2	10	0.2	106	1.4	5.5
D12H-04	m	0.01	0.21	14	1	125	1	1	3	78.1	4.0	4.0	0.3	2	4	0.4	123	0.9	5.1
D12H-05	m	0.01	0.11	14	0	25	0	1	3	40.3	3.4	3.3	0.1	3	15	0.3	168	5.1	5.7
D12H-5.1	bc	0.04	0.25	14	0	72	1	2	3	20.7	5.6	5.4	1.4	4	9	0.3	222	1.3	6.0
D12H-06	m	0.15	0.98	16	1	147	0	2	5	107.6	3.7	3.7	1.7	4	15	0.2	180	1.2	5.5
D12H-6.1	dr	0.02	0.34	14	1	61	1	1	10	51.4	3.6	3.4	5.4	3	13	0.3	90	1.4	5.5
D12H-07	m	0.15	0.23	13	0	70	1	0	2	63.2	3.7	3.8	0.1	1	6	0.2	105	1.1	5.2
D12H-08	r	0.04	1.03	12	1	60	3	45	2	41.6	3.7	3.4	0.2	1	4	0.3	49	1.4	5.9
D12H-010	d	0.19	0.34	12	0	29	1	2	4	37.9	4.2	4.1	0.1	2	13	0.2	89	2.0	5.3
D12H-011	m	0.06	0.35	12	1	69	1	0	2	36.7	2.7	2.5	0.1	1	8	0.2	67	0.9	4.2
D12H-14.1	oc	0.41	2.01	30	1	210	1	31	5	49.9	18.4	18.3	6.4	33	51	0.2	1594	2.9	5.7
D12H-15.1	oc	0.22	0.76	14	1	210	0	2	2	14.6	9.9	9.6	4.7	7	20	0.2	685	5.7	5.4
D12H-17	r	0.03	0.52	15	1	71	1	2	4	40.8	3.1	3.2	2.3	7	5	0.2	83	1.0	4.6
D12H-18	m	0.05	1.36	14	2	88	1	2	3	44.3	3.5	3.4	0.3	1	2	0.3	76	0.9	5.0
D12H-1	*r*	*0.24*	*3.01*	*29*	*4*	*118*	*12*	*1067*	*20*	*56.6*	*4.8*	*4.8*	*6.1*	*18*	*12*	*0.2*	*131*	*1.5*	*6.3*
D12H-09	*oc*	*0.06*	*1.26*	*32*	*3*	*1309*	*1*	*31*	*405*	*118.4*	*7.4*	*7.3*	*1.9*	*38*	*23*	*0.1*	*1921*	*1.8*	*5.1*
D12H-10.1	*br*	*0.10*	*0.53*	*38*	*92*	*38*	*19*	*1301*	*254*	*44.5*	*74.1*	*72.3*	*44.1*	*708*	*1383*	*0.2*	*56*	*1.9*	*5.6*
D12H-012	*r*	*0.09*	*0.19*	*10*	*0*	*48*	*1*	*0*	*2*	*42.2*	*2.7*	*2.4*	*0.1*	*1*	*7*	*0.2*	*65*	*0.9*	*4.8*
D12H-0.13.1	*bc*	*0.45*	*5.69*	*20*	*4*	*237*	*1*	*15*	*42*	*117.9*	*4.7*	*4.7*	*15.7*	*182*	*10*	*0.2*	*234*	*1.1*	*5.2*
D12H-16	*d*	*0.24*	*2.60*	*41*	*4*	*32*	*2*	*34*	*115*	*29.6*	*6.7*	*6.4*	*68.3*	*26*	*82*	*0.2*	*88*	*0.7*	*4.9*
ZD21G-3	m	0.19	0.18	17	0	23	1	0	2	49.7	1.3	1.2	0.1	1	3	0.2	54	0.7	7.5
ZD21G-5	m	0.21	0.26	15	0	30	1	1	3	34.1	1.5	1.4	0.2	2	17	0.2	52	0.7	6.3
ZD21G-8	m	0.28	0.26	15	1	23	1	4	6	44.6	1.9	1.8	0.4	3	25	0.2	55	1.0	6.4
ZD21G-12	m	0.33	0.37	17	1	126	1	2	3	93.3	2.2	2.3	0.2	1	19	0.2	149	0.7	6.7
ZD21G-15	oc	0.58	3.22	17	1	184	0	29	5	36.6	6.6	6.5	3.8	12	41	0.3	526	4.5	6.2
ZD21G-16	d	0.29	0.19	17	0	38	0	3	3	44.9	1.5	1.4	0.1	1	16	0.2	68	0.8	6.6
ZD21G-17	d	0.25	0.20	17	1	47	0	1	3	55.0	1.5	1.3	0.1	11	24	0.2	81	0.9	6.4
ZD21G-19	c	0.22	0.12	16	0	398	1	1	1	113.6	19.1	19.0	17.2	2	7	0.4	864	3.3	6.1
ZD21G-22	d	0.42	0.33	18	1	37	2	18	10	42.5	1.6	1.6	0.2	2	22	0.3	55	0.8	5.6
ZD21G-23	m	0.15	0.22	11	3	26	1	2	13	44.5	1.2	1.3	0.2	61	83	0.2	53	0.8	5.5
ZD21G-25	m	0.20	0.22	24	1	24	0	1	2	35.1	5.9	5.9	0.3	2	13	0.2	34	0.6	8.1
ZD21G-27	m	0.21	0.16	16	0	37	0	2	4	51.0	1.5	1.5	0.1	1	8	0.2	63	0.7	7.0
ZD21G-1	*m*	*0.26*	*0.29*	*26*	*1*	*35*	*0*	*9*	*19*	*45.4*	*3.1*	*3.0*	*1.7*	*12*	*84*	*0.3*	*62*	*0.9*	*8.8*
ZD21G-2	*dr*	*0.60*	*25.05*	*171*	*16*	*77*	*3*	*434*	*908*	*62.4*	*75.1*	*72.9*	*74.9*	*179*	*282*	*0.3*	*428*	*1.9*	*9.4*
ZD21G-4	*bc*	*0.32*	*0.92*	*22*	*35*	*348*	*15*	*691*	*60*	*58.9*	*24.8*	*24.5*	*21.8*	*86*	*557*	*0.2*	*823*	*3.7*	*7.7*
ZD21G-6	*dc*	*0.22*	*0.37*	*12*	*4*	*33*	*1*	*3*	*10*	*65.6*	*3.9*	*3.8*	*2.1*	*42*	*213*	*0.2*	*90*	*0.8*	*6.6*
ZD21G-7	*r*	*0.28*	*0.89*	*23*	*25*	*46*	*4*	*100*	*47*	*49.8*	*14.3*	*13.9*	*19.8*	*151*	*907*	*0.3*	*131*	*1.3*	*7.2*
ZD21G-9	*d*	*0.61*	*13.94*	*109*	*14*	*83*	*4*	*303*	*982*	*61.5*	*53.8*	*53.3*	*122.7*	*263*	*285*	*0.3*	*224*	*1.1*	*6.8*
ZD21G-10	*dr*	*0.24*	*0.48*	*18*	*1*	*35*	*2*	*150*	*21*	*33.1*	*1.8*	*1.8*	*2.1*	*23*	*17*	*0.3*	*55*	*0.9*	*6.2*
ZD21G-11	*m*	*0.38*	*0.36*	*20*	*14*	*36*	*0*	*3*	*9*	*64.1*	*12.2*	*11.9*	*3.2*	*35*	*247*	*0.3*	*92*	*1.0*	*8.5*
ZD21G-13	*d*	*0.30*	*0.71*	*16*	*3*	*27*	*1*	*8*	*26*	*40.2*	*3.8*	*3.8*	*4.8*	*33*	*77*	*0.3*	*64*	*0.9*	*6.3*
ZD21G-14	*dr*	*0.23*	*0.77*	*19*	*3*	*36*	*2*	*37*	*45*	*40.5*	*3.9*	*3.8*	*7.3*	*29*	*31*	*0.2*	*75*	*0.9*	*6.7*
ZD21G-18	*d*	*1.15*	*29.38*	*226*	*43*	*165*	*9*	*299*	*3231*	*97.0*	*189.9*	*187.0*	*397.8*	*670*	*1017*	*0.3*	*761*	*3.2*	*10.8*
ZD21G-20	*d*	*0.38*	*4.13*	*32*	*5*	*35*	*2*	*63*	*259*	*38.9*	*23.7*	*23.9*	*28.5*	*70*	*190*	*0.3*	*88*	*1.2*	*6.3*
ZD21G-21	*m*	*0.18*	*1.00*	*18*	*2*	*62*	*2*	*62*	*100*	*24.8*	*4.3*	*4.0*	*9.8*	*15*	*18*	*0.2*	*168*	*1.5*	*5.6*
ZD21G-24	*m*	*0.64*	*1.33*	*38*	*98*	*48*	*2*	*34*	*74*	*42.3*	*85.4*	*83.4*	*50.6*	*352*	*3386*	*0.4*	*137*	*2.3*	*9.0*
ZD21G-26	*m*	*2.73*	*45.74*	*488*	*50*	*135*	*9*	*1894*	*2839*	*51.6*	*110.8*	*108.7*	*168.3*	*1226*	*545*	*0.7*	*1372*	*5.5*	*10.0*
ZD22A-01	r	0.85	3.54	16	5	149	2	14	44	13.6	10.1	10.2	2.8	50	65	0.2	570	4.0	5.1
ZD22A-3	oc	0.09	0.40	14	1	264	0	1	5	37.3	17.6	17.8	8.9	8	60	0.3	582	5.6	4.9
ZD22A-04	dc	0.28	1.63	18	3	383	1	8	19	29.8	8.1	8.2	3.7	29	49	0.3	931	9.5	5.6
ZD22A-07	oc	0.12	0.52	13	1	416	1	5	7	90.1	13.8	13.4	14.1	5	11	0.3	1063	4.8	5.3
ZD22A-09	r	0.11	0.32	12	1	53	1	1	3	3.1	1.6	1.5	0.2	11	27	0.1	244	3.2	5.3
ZD22A-010	r	0.19	0.20	13	0	233	1	1	2	20.3	3.8	3.7	0.1	5	22	0.2	421	2.9	4.9
ZD22A-011	d	0.12	0.20	11	1	208	1	1	2	21.3	3.1	3.0	0.1	5	25	0.2	383	3.1	5.1
ZD22A-012	c	0.10	0.35	14	1	211	2	0	2	22.8	14.1	13.9	10.8	5	15	0.2	902	2.7	5.1
ZD22A-013	bc	0.03	0.07	11	1	116	1	1	1	39.5	4.8	4.8	0.7	2	3	0.2	160	2.2	4.8
ZD22A-2	*r*	*0.24*	*0.41*	*12*	*5*	*24*	*15*	*2499*	*9*	*33.8*	*15.4*	*13.9*	*9.7*	*28*	*157*	*0.2*	*103*	*1.4*	*6.0*
ZD22A-02	*dc*	*0.88*	*29.06*	*344*	*47*	*446*	*5*	*216*	*2124*	*52.6*	*106.6*	*103.3*	*277.3*	*425*	*774*	*0.3*	*1446*	*9.6*	*7.1*
ZD22A-03	*r*	*0.11*	*0.75*	*32*	*1*	*39*	*1*	*42*	*95*	*17.6*	*4.9*	*4.9*	*11.6*	*27*	*88*	*0.2*	*257*	*2.1*	*5.4*
ZD22A-05	*r*	*0.14*	*0.41*	*18*	*2*	*118*	*8*	*562*	*17*	*27.0*	*3.3*	*3.7*	*7.4*	*24*	*87*	*0.3*	*278*	*2.6*	*5.8*
ZD22A-06	*d*	*0.84*	*33.30*	*63*	*33*	*660*	*7*	*176*	*366*	*87.8*	*28.9*	*29.1*	*120.0*	*357*	*149*	*0.2*	*1249*	*7.4*	*6.6*
ZD22A-08	*d*	*0.18*	*0.58*	*20*	*1*	*370*	*1*	*304*	*23*	*44.8*	*4.9*	*4.8*	*8.0*	*7*	*30*	*0.3*	*658*	*8.6*	*5.1*
CZ3-5.1		0.02	0.79	25	1.2	13	1.2	1.7	1.0	4.7	7.4	7.3	1.2	1.47	1.16	0.4	42.7	0.5	1.2
CZ3-5.4		0.02	0.78	13	0.8	12	1.2	0.0	0.5	4.1	6.5	6.2	0.6	0.45	0.62	0.3	42.2	0.6	0.9
CZ3-5.6		0.02	0.63	12	1.0	13	0.7	0.0	1.3	4.0	6.3	6.5	1.0	1.41	0.96	0.2	42.0	0.5	0.8
CZ3-6.2		0.02	0.73	16	0.9	13	0.6	1.6	0.7	4.8	7.6	7.5	1.1	0.62	0.88	0.4	47.2	0.5	1.2
CZ3-6.3		0.02	0.58	13	1.1	13	1.0	0.9	1.2	5.3	8.5	8.7	1.2	1.21	1.20	0.3	51.5	0.6	1.0
CZ3-6.4		0.01	0.63	10	0.9	13	1.2	1.8	1.3	4.2	6.2	6.5	0.8	0.83	0.69	0.3	41.4	0.5	1.0
CZ3 Ave.		0.02	0.69	15	1	13	1	1	1	4.5	7.1	7.1	1	1	0.92	0.3	44.5	0.6	1

Note: Analyses performed 16-17 March 2007. Samples in italics show probable non-zircon contamination (see text). Abbreviations of CL textures: c, medium CL core; d, dark CL grain; m, medium CL grain; r, medium CL rim; bc, bright CL core; dc, dark CL core; dr, dark CL rim; oc, oscillatory zoned core.

Table 2: (continued)

analysis	CL	La	Ce	Nd	Sm	Eu	Gd	Tb	Dy	Ho	Er	Tm	Yb	Lu	Hf	Th	U	Th/U	Ce/ Ce*	Eu/ Eu*	Yb/ Gd	T(°C) (^{48}Ti)	T(°C) (^{49}Ti)
D12H-2	m	0.147	0.79	0.15	0.56	0.49	9.21	3.56	28.4	6.82	22.8	3.7	25.5	4.2	15959	2.7	530	0.005	3	0.66	2.8	668	666
D12H-3	d	0.108	1.23	0.17	0.77	0.65	9.21	2.49	18.1	4.29	14.7	2.5	18.8	3.3	15680	7.0	729	0.010	5	0.74	2.0	696	698
D12H-04	m	0.028	0.33	0.03	0.26	0.29	4.70	2.02	16.4	4.18	12.7	2.1	14.0	2.3	11944	0.6	162	0.004	6	0.81	3.0	662	663
D12H-05	m	0.034	0.61	0.02	0.14	0.09	2.55	1.56	19.0	6.02	24.2	4.5	29.2	4.6	17178	2.2	867	0.003	10	0.45	11.5	650	648
D12H-5.1	bc	0.031	6.44	0.25	0.63	0.20	6.00	2.15	24.6	9.33	47.8	9.2	84.6	16.8	10474	23.3	70	0.335	50	0.31	14.1	689	685
D12H-06	m	0.620	1.15	0.21	0.42	0.32	6.51	2.86	26.4	7.37	26.9	4.9	34.2	5.8	15739	1.6	377	0.004	1	0.59	5.2	657	657
D12H-6.1	dr	5.44	3.80	1.59	1.23	0.48	7.46	1.99	15.3	3.80	11.7	2.0	13.9	2.4	15160	3.9	915	0.004	1	0.48	1.9	656	652
D12H-07	m	0.027	0.59	0.06	0.47	0.34	7.77	2.22	17.7	4.05	14.1	2.3	16.8	2.6	15840	5.2	612	0.009	8	0.54	2.2	657	660
D12H-08	r	0.084	1.20	0.08	0.36	0.35	4.92	1.23	9.3	1.96	6.4	1.0	7.4	1.2	15938	5.5	942	0.006	7	0.80	1.5	657	652
D12H-010	d	0.086	0.91	0.06	0.25	0.19	3.74	1.47	11.2	3.12	9.4	1.8	12.2	1.8	14328	4.8	760	0.006	6	0.59	3.3	666	666
D12H-011	m	0.017	0.71	0.05	0.28	0.25	3.75	1.13	8.5	2.04	6.6	1.2	8.1	1.3	10037	2.0	373	0.005	14	0.72	2.1	635	629
D12H-14.1	oc	0.918	14.06	8.37	12.03	1.12	86.01	24.32	221.8	72.24	314.7	60.1	465.0	79.8	9838	307.6	774	0.398	4	0.11	5.4	793	793
D12H-15.1	oc	0.061	19.07	0.52	1.44	0.12	15.77	5.87	67.3	26.96	124.9	26.3	203.8	37.4	11950	124.6	350	0.356	74	0.08	12.9	736	733
D12H-17	r	1.63	3.21	0.53	0.65	0.38	4.81	1.42	10.9	2.90	8.1	1.6	10.5	2.0	9743	4.1	548	0.008	1	0.65	2.2	645	646
D12H-18	m	0.011	0.73	0.10	0.38	0.31	4.70	1.38	9.8	2.41	8.4	1.7	11.2	2.0	10300	3.1	347	0.009	16	0.71	2.4	654	650
D12H-1	*r*	*2.97*	*4.50*	*0.83*	*1.09*	*0.69*	*9.86*	*3.10*	*22.2*	*5.60*	*18.1*	*3.3*	*20.2*	*3.6*	*15408*	*5.1*	*811*	*0.006*	*1*	*0.64*	*2.0*	*677*	*677*
D12H-09	*oc*	*0.428*	*1.62*	*1.14*	*3.60*	*0.18*	*41.17*	*15.99*	*174.5*	*74.15*	*309.2*	*62.3*	*475.3*	*85.7*	*11288*	*61.4*	*322*	*0.191*	*1*	*0.05*	*11.5*	*711*	*710*
D12H-10.1	*br*	*3.62*	*3.23*	*0.61*	*0.49*	*0.23*	*2.32*	*0.73*	*6.5*	*1.96*	*6.6*	*1.2*	*9.3*	*2.0*	*10807*	*1.2*	*134*	*0.009*	*1*	*0.67*	*4.0*	*948*	*945*
D12H-012	*r*	*0.015*	*0.68*	*0.04*	*0.22*	*0.19*	*2.79*	*0.78*	*5.5*	*2.04*	*4.8*	*0.9*	*5.1*	*1.3*	*8843*	*3.2*	*373*	*0.009*	*15*	*0.73*	*1.8*	*633*	*625*
D12H-0.13.1	*bc*	*4.58*	*8.57*	*2.08*	*1.75*	*0.68*	*8.21*	*3.00*	*29.8*	*8.96*	*32.7*	*6.5*	*45.3*	*7.9*	*11960*	*4.3*	*110*	*0.039*	*1*	*0.54*	*5.5*	*675*	*675*
D12H-16	*d*	*24*	*29.50*	*7.62*	*4.26*	*1.09*	*10.79*	*2.41*	*15.0*	*3.09*	*7.8*	*1.2*	*7.6*	*1.2*	*10318*	*2.7*	*744*	*0.004*	*1*	*0.49*	*0.7*	*703*	*700*
ZD21G-3	m	0.022	0.46	0.02	0.25	0.22	3.82	1.06	8.4	1.98	7.1	1.3	9.1	1.5	14774	1.9	591	0.003	10	0.67	2.4	585	583
ZD21G-5	m	0.123	0.47	0.05	0.15	0.13	2.26	0.82	6.2	1.67	5.4	0.9	7.2	1.3	11432	1.7	324	0.005	3	0.70	3.2	594	589
ZD21G-8	m	0.627	0.63	0.33	0.29	0.24	3.45	1.11	8.7	2.06	7.6	1.2	10.2	1.6	14336	1.1	535	0.002	1	0.73	3.0	609	607
ZD21G-12	m	0.053	0.59	0.04	0.29	0.30	5.50	2.57	20.2	5.37	17.3	2.9	20.0	2.9	13319	2.7	635	0.004	6	0.71	3.6	620	623
ZD21G-15	oc	0.590	14.01	0.42	1.04	0.21	13.21	5.06	60.0	23.58	125.2	29.3	264.5	54.2	14909	161.0	664	0.243	13	0.17	20.0	701	701
ZD21G-16	d	0.030	0.49	0.04	0.27	0.23	4.51	1.31	9.6	2.32	8.3	1.4	9.2	1.6	12792	3.7	689	0.005	7	0.63	2.0	595	592
ZD21G-17	d	0.017	0.64	0.06	0.42	0.38	6.88	1.78	12.7	3.03	10.3	1.8	12.3	2.0	15310	4.1	747	0.006	12	0.68	1.8	596	588
ZD21G-19	c	0.059	29.49	0.79	2.09	0.66	23.90	8.73	104.9	39.32	198.3	42.5	354.6	66.5	13105	112.0	142	0.791	102	0.29	14.8	797	796
ZD21G-22	d	0.094	0.44	0.04	0.18	0.19	2.94	0.94	6.8	1.68	6.2	1.1	7.6	1.2	10837	1.8	630	0.003	3	0.78	2.6	599	598
ZD21G-23	m	0.013	0.40	0.02	0.22	0.21	3.84	1.12	8.4	2.06	7.4	1.2	9.2	1.5	13967	1.8	535	0.003	13	0.69	2.4	580	584
ZD21G-25	m	0.034	0.47	0.02	0.16	0.11	1.91	0.59	4.5	1.07	4.3	0.7	5.3	0.9	12246	1.2	318	0.004	8	0.63	2.8	693	693
ZD21G-27	m	0.046	0.49	0.02	0.25	0.25	4.91	1.37	9.9	2.42	7.8	1.4	10.2	1.7	13589	2.4	692	0.004	7	0.70	2.1	595	593
ZD21G-1	*m*	*1.38*	*2.33*	*0.60*	*0.59*	*0.39*	*5.61*	*1.37*	*11.0*	*2.57*	*9.0*	*1.5*	*10.6*	*2.0*	*15445*	*7.3*	*717*	*0.010*	*1*	*0.65*	*1.9*	*643*	*641*
ZD21G-2	*dr*	*171*	*81.69*	*53.41*	*25.18*	*7.27*	*50.53*	*9.77*	*63.8*	*16.11*	*47.1*	*8.0*	*50.7*	*8.7*	*15739*	*34.5*	*1633*	*0.021*	*0*	*0.62*	*1.0*	*950*	*946*
ZD21G-4	*bc*	*5.23*	*47.89*	*4.07*	*4.73*	*1.74*	*25.21*	*7.55*	*71.7*	*29.54*	*117.6*	*24.1*	*191.9*	*37.7*	*8149*	*85.3*	*102*	*0.840*	*5*	*0.49*	*7.6*	*823*	*822*
ZD21G-6	*dc*	*1.30*	*1.47*	*0.41*	*0.45*	*0.29*	*5.65*	*1.66*	*13.2*	*3.14*	*10.3*	*2.0*	*13.1*	*2.5*	*12809*	*2.8*	*873*	*0.003*	*1*	*0.55*	*2.3*	*661*	*659*
ZD21G-7	*r*	*8.00*	*8.04*	*2.76*	*1.82*	*0.62*	*8.19*	*2.35*	*19.2*	*5.80*	*23.8*	*4.7*	*39.9*	*7.5*	*13321*	*18.1*	*357*	*0.051*	*1*	*0.48*	*4.9*	*769*	*767*
ZD21G-9	*d*	*76*	*58.36*	*19.70*	*7.39*	*2.07*	*16.89*	*3.37*	*23.2*	*5.67*	*17.0*	*3.2*	*21.4*	*3.5*	*11417*	*7.4*	*914*	*0.008*	*1*	*0.56*	*1.3*	*909*	*908*
ZD21G-10	*dr*	*3.58*	*3.46*	*2.62*	*1.52*	*0.54*	*6.25*	*1.30*	*9.4*	*2.12*	*6.7*	*1.2*	*7.3*	*1.2*	*15511*	*2.1*	*894*	*0.002*	*1*	*0.53*	*1.2*	*608*	*607*
ZD21G-11	*m*	*0.376*	*1.13*	*0.26*	*0.49*	*0.45*	*7.01*	*1.85*	*13.5*	*3.25*	*11.1*	*2.0*	*12.6*	*2.1*	*13690*	*3.8*	*664*	*0.006*	*2*	*0.74*	*1.8*	*755*	*752*
ZD21G-13	*d*	*3.76*	*4.90*	*1.46*	*0.92*	*0.43*	*5.51*	*1.45*	*11.0*	*2.40*	*9.8*	*1.7*	*12.0*	*2.1*	*15546*	*2.1*	*551*	*0.004*	*1*	*0.58*	*2.2*	*660*	*659*
ZD21G-14	*dr*	*5.97*	*6.90*	*1.98*	*0.97*	*0.44*	*5.61*	*1.68*	*12.1*	*3.19*	*10.7*	*2.2*	*17.7*	*3.8*	*15590*	*6.1*	*680*	*0.009*	*1*	*0.57*	*3.2*	*661*	*659*
ZD21G-18	*d*	*457*	*307*	*125*	*49.10*	*13.37*	*109.51*	*22.45*	*153.2*	*30.04*	*108.7*	*21.0*	*145.9*	*25.2*	*17120*	*131.2*	*1751*	*0.075*	*1*	*0.55*	*1.3*	*1081*	*1079*
ZD21G-20	*d*	*26*	*25.41*	*6.62*	*2.84*	*0.85*	*8.15*	*1.95*	*13.9*	*3.06*	*9.6*	*1.9*	*12.3*	*2.1*	*16485*	*5.9*	*613*	*0.010*	*1*	*0.54*	*1.5*	*818*	*819*
ZD21G-21	*m*	*14*	*11.89*	*3.50*	*1.54*	*0.47*	*7.25*	*2.24*	*21.6*	*7.02*	*29.1*	*6.2*	*48.2*	*8.5*	*12245*	*7.5*	*202*	*0.037*	*1*	*0.43*	*6.7*	*669*	*662*
ZD21G-24	*m*	*5.60*	*6.06*	*2.28*	*1.94*	*0.73*	*8.76*	*2.36*	*17.1*	*4.82*	*17.6*	*3.4*	*26.0*	*5.2*	*11551*	*10.2*	*420*	*0.024*	*1*	*0.54*	*3.0*	*967*	*963*
ZD21G-26	*m*	*320*	*264*	*130*	*83.10*	*25.39*	*175.36*	*37.24*	*254.3*	*66.14*	*205.2*	*37.0*	*252.5*	*38.8*	*15098*	*190.9*	*1058*	*0.180*	*1*	*0.64*	*1.4*	*1002*	*999*
ZD22A-01	r	1.20	12.87	1.22	1.77	1.73	14.46	5.52	63.6	24.41	126.1	29.2	251.2	47.1	14154	131.3	673	0.195	5	1.04	17.4	738	739
ZD22A-3	oc	0.226	78.09	1.73	2.86	1.01	20.88	6.31	65.6	23.02	108.8	24.2	208.8	40.2	10777	64.2	88	0.728	85	0.40	10.0	789	790
ZD22A-04	dc	0.247	21.49	0.55	1.35	3.37	13.28	5.82	76.5	34.91	201.4	55.1	562.9	115.4	15271	157.3	838	0.188	32	2.42	42.4	719	720
ZD22A-07	oc	0.055	58.77	1.16	2.84	1.09	29.45	10.35	122.1	47.68	236.2	51.0	424.1	80.2	13360	145.3	181	0.803	186	0.36	14.4	766	763
ZD22A-09	r	0.180	1.15	0.09	0.14	0.08	1.55	0.75	12.2	6.94	55.6	18.5	233.0	63.8	12521	7.4	544	0.014	4	0.54	150.5	600	597
ZD22A-010	r	0.034	1.33	0.03	0.15	0.14	2.88	1.72	29.2	12.69	66.5	16.5	144.2	28.0	10024	3.9	457	0.008	20	0.66	50.1	659	657
ZD22A-011	d	0.068	3.78	0.07	0.23	0.19	4.09	2.35	32.8	13.52	74.7	19.3	189.9	37.7	13073	23.5	666	0.035	27	0.59	46.4	644	642
ZD22A-012	c	0.063	9.74	0.84	2.39	0.40	27.27	9.40	105.8	40.15	187.7	38.5	311.8	56.1	12638	69.4	216	0.322	32	0.15	11.4	768	766
ZD22A-013	bc	0.027	13.68	0.22	0.55	0.10	4.94	1.61	16.9	6.67	27.8	5.6	41.6	8.5	10180	61.0	25	2.452	120	0.19	8.4	676	677
ZD22A-2	*r*	*2.36*	*2.07*	*0.44*	*0.46*	*0.32*	*4.11*	*1.32*	*10.6*	*3.25*	*10.8*	*1.9*	*15.8*	*2.7*	*9693*	*2.5*	*344*	*0.007*	*1*	*0.72*	*3.8*	*776*	*766*
ZD22A-02	*dc*	*125*	*217*	*89.28*	*68.12*	*21.63*	*168.17*	*36.38*	*248.9*	*67.55*	*292.7*	*60.2*	*475.8*	*82.0*	*15593*	*881.2*	*1032*	*0.854*	*1*	*0.61*	*2.8*	*996*	*992*
ZD22A-03	*r*	*6.56*	*11.65*	*3.84*	*3.03*	*1.04*	*11.42*	*3.26*	*30.4*	*10.29*	*55.8*	*13.1*	*121.4*	*27.2*	*14767*	*56.1*	*723*	*0.078*	*1*	*0.54*	*10.6*	*678*	*679*
ZD22A-05	*r*	*2.10*	*4.03*	*0.57*	*0.68*	*0.34*	*4.86*	*2.28*	*28.3*	*11.32*	*63.7*	*15.2*	*134.6*	*26.4*	*14110*	*8.1*	*625*	*0.013*	*1*	*0.56*	*27.7*	*648*	*657*
ZD22A-06	*d*	*27*	*128*	*18.72*	*14.18*	*6.37*	*49.12*	*14.42*	*136.1*	*48.74*	*252.3*	*65.3*	*671.6*	*137.1*	*13906*	*131.4*	*1117*	*0.118*	*3*	*0.73*	*13.7*	*839*	*839*
ZD22A-08	*d*	*4.18*	*9.20*	*2.26*	*1.45*	*0.65*	*7.50*	*3.18*	*51.9*	*26.11*	*156.0*	*41.9*	*376.2*	*71.8*	*15167*	*5.0*	*737*	*0.007*	*1*	*0.60*	*50.2*	*679*	*677*
CZ3-5.1		0.039	0.51	0.07	0.11	0.044	0.76	0.42	4.6	1.71	8.3	1.8	15.1	2.5	11434	24	463	0.052	5	0.47	20.0	712	710
CZ3-5.4		0.042	0.52	0.04	0.12	0.050	0.82	0.40	4.9	1.93	7.6	1.9	14.6	2.7	14050	36	642	0.057	6	0.49	17.7	701	697
CZ3-5.6		0.038	0.48	0.08	0.12	0.041	0.82	0.34	4.1	1.75	8.1	1.8	14.7	2.5	13198	32	607	0.052	5	0.40	17.8	698	701
CZ3-6.2		0.022	0.49	0.07	0.11	0.052	1.32	0.42	5.3	2.02	9.6	2.0	18.3	2.9	13577	32	601	0.053	7	0.43	13.9	713	713
CZ3-6.3		0.026	0.52	0.06	0.15	0.053	1.11	0.42	5.5	1.89	8.8	2.0	15.9	2.7	11891	27	506	0.053	7	0.40	14.3	723	724
CZ3-6.4		0.020	0.42	0.05	0.12	0.054	0.92	0.29	3.8	1.74	7.3	1.4	12.1	2.3	11450	26	482	0.055	7	0.49	13.1	698	700
CZ3 Ave.		0.031	0.49	0.06	0.12	0.049	0.96	0.38	4.7	1.84	8.3	1.8	15.1	2.6	12600	30	550	0.054	6	0.44	15.7	708	708

Note: Samples in italics show probable non-zircon contamination (see text). Abbreviations of CL textures: c, medium CL core; d, dark CL grain; m, medium CL grain; r, medium CL rim; bc, bright CL core; dc, dark CL core; dr, dark CL rim; oc, oscillatory zoned core.

Table 3

Table 3: Garnet and plagioclase trace element data, paragneiss samples D12H, ZD21G, and ZD22A, North Qaidam terrane, western China. Concentrations in ppm.

analysis	Li	Mg	Ca	Sc	Ti	V	Cr	Rb	Sr	Y	Zr	Nb	Ba
garnet													
D12h-1	7.1	19016	17868	100	89	22	52	0.039	0.075	260	1.56	0.0067	<0.037
D12h-1-2	11	19431	17868	108	120	25	50	0.042	0.100	273	2.24	<0.0054	0.094
D12h-1-3	12	19951	15723	105	112	30	134	0.095	0.128	257	1.96	0.0074	0.242
D12h-1-4	28	20877	15723	109	60	26	43	0.09	0.095	257	1.36	<0.0043	0.38
D12h-1-5	28	18605	13579	98	18	18	42	0.078	0.103	308	0.53	0.0214	0.54
D12h-1-6	19	13956	13579	76	36	15	39	0.065	0.112	202	0.76	0.007	0.359
D12h-1-7	18	22521	17868	121	121	35	121	0.204	0.166	275	2.22	<0.0071	0.357
D12h-1-8	8.9	19355	17868	101	109	29	54	0.128	0.161	227	1.76	<0.0041	0.41
D12h-1-9	14	19228	17868	101	105	19	15	0.229	0.170	251	1.84	0.0043	0.68
D12h-2-1	12	18422	17868	97	93	26	38	0.038	0.079	232	1.91	<0.0049	<0.042
D12h-2-2	21	17972	16438	94	108	29	60	0.028	0.088	222	2.03	<0.0043	0.054
D12h-2-3	25	16730	13579	81	55	26	45	0.033	0.069	212	1.78	<0.0038	0.071
D12h-2-4	21	18840	13579	105	83	25	57	0.079	0.084	270	1.61	<0.0048	0.08
D12h-2-6	28	20470	15009	106	74	28	63	0.064	0.093	280	1.92	<0.0036	0.103
D12h-2-7	11	17640	16438	92	102	28	76	0.144	0.154	219	2.60	0.0116	0.38
D12h-2-8	12	19645	17868	92	98	34	131	0.091	0.127	225	1.74	<0.0058	0.121
ZD21gg1-1	31	31255	36451	132	127	29	76	0.06	0.042	469	1.42	0.081	<0.049
ZD21gg1-2	23	17659	26445	92	208	26	47	0.048	0.039	388	1.40	0.11	0.014
ZD21gg1-3	39	13495	26445	65	274	50	35	0.189	0.095	1696	0.59	0.006	<0.030
ZD21gg1-4	64	16839	35736	101	472	51	67	0.254	0.115	1802	2.27	0.8	<0.0311
ZD21gg1-5	194	16620	35736	304	436	67	118	1.33	1.250	4779	1.36	0.173	<0.038
ZD21gg1-6	101	12166	29303	211	278	58	90	0.64	0.402	3430	11.3	0.0228	<0.042
ZD21gg1-7	72	12600	31448	144	371	54	86	0.364	0.246	2563	1.12	0.039	<0.030
ZD21gg1-8	36	14736	28589	122	288	31	65	0.158	0.084	951	1.15	0.053	<0.033
ZD21gg1-9	21	23218	30018	131	231	27	103	0.181	0.051	426	1.56	<0.0071	0.148
ZD21gg110	17	17903	46457	89	468	62	147	0.021	0.035	135	3.05	<0.0049	<0.028
ZD21gg111	22	23019	46457	100	247	53	154	0.05	0.041	250	5.59	0.028	<0.0240
ZD21gg112	22	20851	46457	90	540	45	235	0.034	0.031	208	7.89	0.279	<0.028
ZD21gg113	16	20975	46457	86	550	43	112	0.029	0.036	211	8.71	<0.0045	<0.038
ZD21gg2-1	37	14920	15724	75	27	35	119	1.89	1.070	427	1.55	0.03	0.09
ZD21gg3-1	14	11634	25015	56	298	32	55	0.035	0.019	149	5.18	0.57	0.039
ZD21gg3-2	9.4	10695	25015	48	311	33	209	0.014	0.020	128	2.84	0.0017	<0.0166
ZD21gg3-3	14	14643	25015	58	157	30	144	0.024	0.028	171	2.04	<0.0027	<0.023
ZD21gg3-4	25	17233	21442	70	17	18	48	0.017	0.032	96	1.14	<0.0046	0.113
plagioclase													
ZD21g-p2	79	1167	28589	2.4	224	2.2	18	227	884	1.5	0.22	0.8	1733

Note: Analyses performed 3-4 August 2006. Detection limits calculated by Glitter software.

Table 3: (continued)

analysis	La	Ce	Pr	Nd	Sm	Eu	Gd	Tb	Dy	Ho	Er	Tm	Yb	Lu	Hf	Eu/Eu*	Yb/Gd
garnet																	
D12h-1	<0.0015	0.008	0.012	0.263	1.67	1.38	15	6.3	53	12.4	36	5.4	37	5.5	0.037	0.84	3.1
D12h-1-2	0.0035	0.009	0.009	0.246	1.61	1.25	14	5.8	49	11.4	34	4.8	32	4.7	0.040	0.81	2.9
D12h-1-3	0.0062	0.027	0.008	0.227	1.37	1.16	14	5.9	48	10.7	31	4.6	30	4.5	0.032	0.82	2.7
D12h-1-4	0.0051	0.019	0.008	0.105	1.22	1.17	15	5.4	46	10.9	32	4.7	31	4.6	0.019	0.84	2.6
D12h-1-5	0.005	0.017	0.005	0.084	0.61	0.72	12	6.8	59	13.4	38	5.6	36	5.4	0.013	0.80	3.7
D12h-1-6	0.0066	0.021	0.007	0.105	2.17	2.74	34	7.5	42	8.4	24	3.5	23	3.3	0.011	0.97	0.8
D12h-1-7	0.0067	0.018	0.011	0.234	1.48	1.27	14	6.2	50	11.3	32	4.8	32	4.7	0.034	0.84	2.7
D12h-1-8	0.0082	0.030	0.008	0.222	1.46	1.2	13	5.3	41	9.2	26	3.8	24	3.6	0.029	0.83	2.2
D12h-1-9	0.0078	0.040	0.014	0.249	1.44	1.17	13	5.3	44	10.2	30	4.5	29	4.3	0.027	0.84	2.9
D12h-2-1	<0.00134	0.005	0.010	0.231	1.44	1.17	13	5.1	44	9.7	28	4.0	26	3.7	0.031	0.83	2.5
D12h-2-2	<0.00138	0.009	0.005	0.215	1.43	1.10	12	5.1	41	9.4	28	4.1	27	4.1	0.035	0.80	2.7
D12h-2-3	<0.00112	0.007	0.003	0.164	0.91	0.83	10	4.6	38	9.0	26	3.9	26	3.8	0.029	0.83	3.1
D12h-2-4	0.00153	0.013	0.007	0.149	1.13	0.96	12	5.7	49	11.4	33	4.9	33	4.8	0.026	0.79	3.4
D12h-2-6	0.0056	0.012	0.005	0.155	1.14	0.95	12	5.6	49	11.7	34	5.1	34	5.0	0.020	0.79	3.5
D12h-2-7	0.0062	0.036	0.010	0.188	1.45	1.11	12	5.0	41	9.2	27	4.0	26	3.9	0.043	0.80	2.6
D12h-2-8	0.0045	0.035	0.007	0.185	1.42	1.13	13	5.3	44	9.8	28	4.0	25	3.7	0.035	0.81	2.4
ZD21gg1-1	<0.0030	0.006	0.006	0.217	2.5	2.06	26	10.3	89	21.0	60	8.2	48	6.6	0.027	0.77	2.3
ZD21gg1-2	0.0018	0.005	0.005	0.203	2.48	2.38	27	9.2	73	16.5	48	6.9	41	5.7	0.020	0.89	1.9
ZD21gg1-3	0.00239	0.002	0.002	0.129	1.61	1.47	29	19.2	243	65.0	188	25.4	137	16.7	0.016	0.66	5.9
ZD21gg1-4	0.006	0.015	0.007	0.186	1.71	1.35	23	15.3	218	70.3	233	35.0	207	27.9	0.044	0.65	10.9
ZD21gg1-5	0.0026	0.009	0.003	0.082	0.99	0.79	16	15.1	360	204	1207	292	2500	397	0.035	0.61	194.8
ZD21gg1-6	0.0032	0.007	0.003	0.104	1.1	1	19	16.8	321	131	568	103	706	99.7	0.341	0.67	46.1
ZD21gg1-7	<0.00164	0.005	0.004	0.154	2.12	1.92	37	26.2	340	101	339	52.9	321	43.1	0.032	0.66	10.6
ZD21gg1-8	<0.00154	0.005	0.005	0.221	2.76	2.41	33	15.5	160	41.5	129	18.9	118	16.5	0.032	0.77	4.4
ZD21gg1-9	<0.00240	0.004	0.005	0.158	1.83	1.72	21	8.3	76	19.6	64	10.0	66	10.0	0.029	0.85	3.9
ZD21gg110	<0.0018	0.017	0.021	0.617	3.84	2.72	26	5.6	30	4.8	12	1.5	9.5	1.3	0.037	0.83	0.5
ZD21gg111	<0.0017	0.019	0.015	0.363	2.96	2.17	24	6.8	47	9.6	27	3.9	26	3.9	0.077	0.78	1.3
ZD21gg112	<0.00139	0.023	0.019	0.66	4.18	2.75	26	6.3	40	7.9	23	3.4	23	3.7	0.113	0.80	1.1
ZD21gg113	<0.00124	0.023	0.024	0.69	4.4	2.92	26	6.1	39	7.9	23	3.5	23	3.6	0.121	0.82	1.1
ZD21gg2-1	0.064	0.032	0.027	0.118	0.63	0.4	10	4.9	57	17.2	58	8.8	55	8.7	0.029	0.49	6.9
ZD21gg3-1	0.00153	0.013	0.009	0.317	2.28	1.52	16	4.0	27	5.6	16	2.3	15	2.2	0.065	0.77	1.2
ZD21gg3-2	0.00356	0.017	0.016	0.395	2.49	1.64	15	3.7	24	4.7	13	1.8	11	1.5	0.036	0.81	0.9
ZD21gg3-3	<0.00098	0.008	0.013	0.38	2.92	2.03	22	5.4	33	6.1	16	2.2	14	2.0	0.029	0.78	0.8
ZD21gg3-4	0.00205	0.007	0.002	0.06	0.61	0.42	7.5	2.2	16	3.3	8.9	1.3	8.1	1.1	0.017	0.60	1.3
plagioclase																	
ZD21g-p2	2.06	4.0	0.399	1.29	0.28	5.56	0.267	0.047	0.239	0.051	0.166	0.026	0.212	0.027	0.030	62.0	1.0

Note: Analyses performed 3-4 August 2006. Detection limits calculated by Glitter software.